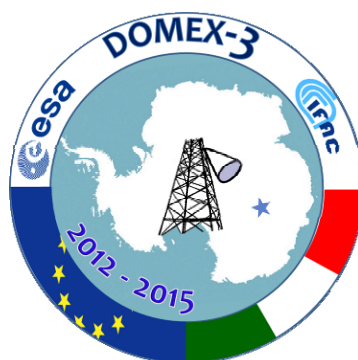


Technical Support for the Long-Term Deployment of an L-Band Radiometer at Concordia Station

Yearly Report – Data Acquisition and Processing Report
Second Year – D3- D6
June 2015

EUROPEAN SPACE AGENCY STUDY
ESTEC Contract 4000105872/12/NL/NF



Prepared by

Giovanni MACELLONI, Marco BROGIONI, Simone Pettinato, Francesco Montomoli
IFAC- CNR, Florence, ITALY

DATE: 13/6/2015

Version: 1.0

Deliverable of the contract: D6



Consiglio Nazionale delle Ricerche
Istituto di Fisica Applicata "Nello Carrara"
VIA MADONNA DEL PIANO N. 10 - CAP 50019 SESTO FIORENTINO FIRENZE

This page is intentionally left blank

ESA STUDY CONTRACT REPORT

ESTEC CONTRACT NO: 4000105872/12/NL/NF	SUBJECT: Technical Support for the Long-Term Deployment of an L-Band Radiometer at Concordia Station	CONTRACTOR: IFAC
ESA CR ()No:	STAR CODE:	No of volumes: 1 This is volume no: 1
		CONTRACTOR'S REF: Deliverable
<p>ABSTRACT:</p> <p>This document is related to Task2 (Deliverable D6) of the study <i>Technical Support for the Long-Term Deployment of an L-Band Radiometer at Concordia Station</i> (ESTEC contract 4000105872/12/NL/NF). It contains the Second Year Report of the Domex-3 Experiment. In the document is described the execution of the activity were carried out in the second experimental year of the project (i.e. form November 2013 to November 2014) It includes the description of the second summer campaign 2013-2014 as well as the activity was conducted during first year of the winter campaign and in Italy. Data analysis and Data Processing Report is also reported here.</p>		
<p>The work described in this report was done under ESA Contract. Responsibility for the contents resides in the authors or organisation that prepared it.</p>		
<p>PREPARED BY:</p> <p>GIOVANNI MACELLONI, MARCO BROGIONI, SIMONE PETTINATO, FRANCESCO MONTOMOLI -IFAC</p>		
ESA STUDY MANAGER: TANIA CASAL	ESA BUDGET HEADING:	

DOCUMENT CHANGE LOG

Issue/ Revision	Date	Observations
1/0	13/06/2015	First issue –Draft Version

ABBREVIATIONS

AEP	Annual Executive Project
AWS	Automatic Weather Station
CVA-ARABBA	Avalanche Center of Arabba, Italy
ESA	European Space Agency
IASH	International Association of Scientific Hydrology
IFAC-CNR	Institute of Applied Physics – National Research Council
INGV	Istituto Nazionale di Geofisica e Vulcanologia
IOP	Intensive Operational Period
MZS	Mario Zucchelli Station
NOP	Normal Operational Period
OMT	OrthoMode Transducer
PNRA	Programma Nazionale Ricerche in Antartide
RFI	Radio Frequency Interference
RR	Readiness Review Document – D1 of the contract
TEC	Total Electron Content

This page is intentionally left blank.

TABLE OF CONTENTS

1	PURPOSE AND STRUCTURE OF DOCUMENT.....	9
2	OVERVIEW	11
3	THE 2013 SUMMER ANTARCTIC CAMPAIGN	12
3.1	Description of the campaign.....	12
3.2	Activity with the winterover researchers	17
4	2014 WINTER PERIOD	19
4.1	Radiometer acquisition.....	19
4.2	Snow activities	20
4.3	2014 Activity at IFAC.....	20
4.3.1	Preparation of material for 2014 summer campaign.....	20
4.3.2	Preparation for the 2014 summer campaign	22
4.3.3	Theoretical Modelling of DOMEX data.....	24
5	DOMEX-3 - 2014 DATA ANALYSIS	46
5.1	RADOMEX data	46
5.1.1	DATA PROCESSING	46
5.1.2	DATA ANALYSIS	56
5.2	Comparison to SMOS data.....	64
5.3	SNOW Data	65
5.3.1	Snow temperature	65
6	REFERENCES.....	68

This page is intentionally left blank.

1 Purpose and structure of document

Purpose

This document contains the Second Year Report for DOMEX-3 experiment, prepared by the Institute for Applied Physics “Nello Carrara” – Firenze within the framework of the ESA contract N. 4000105872/12/NL/NF.

In the document is described the execution of the activity were carried out in the first experimental year of the project (i.e. form November 2013 to November 2014) It includes the description of the second summer campaign 2013-2014 as well as the activity was conducted during second year of the winter campaign and in Italy.

The document is divided into sections in which the individual points were discussed.

This page is intentionally left blank.

2 Overview

The Domex-3 experiment is the follow on of two previous experiments called Domex-1 and Domex-2 which were successfully conducted at Concordia base, Antarctica, by IFAC-CNR in cooperation to the Agency (contracts N. 18060/04/NL/CB [1] and N. 22046/08/NL/EL, 20066/06/NL/EL [2]) and PNRA.

The results obtained in these contracts demonstrated that DOME- C represents a unique “high”-temperature, extended target that provides a temporally stable reference, which potentially meets existing requirements for assessing the long-term stability of space-borne L-band radiometric instruments.

In order to meet this objective, co-located ground measurements are required in order to verify target stability over time and to monitor changes in target characteristics that may affect the long-term reference signal: for example, surface roughness or “crusting”, which in spite of being quite stable, appears to evolve with time (possibly due to climatic changes) and may affect the brightness temperature. Long-term monitoring of DOME-C is also crucial to investigating further and to modeling the Tb variations observed in H-pol during the DOMEX-2 experiment. A long-term experiment is also recommended in order to provide a continuous data record of ground-based radiometric measurements covering the SMOS – Aquarius – SMAP era. The resulting data set will support the Level 1C quality assessment for SMOS and SMAP at the accuracy level required for climate applications. In addition, the produced data set will be instrumental for satellite sensor product intercalibration ensuring a harmonized Level 1 data set of passive microwave observations at L-band for future climate applications.

The objective of DOMEX-3 project is to contribute to the long-term deployment of an L-Band Radiometer at Concordia Station. The activity of the contract is divided in five phases: the first phase deals with the preparation of the instrument and the experiment while the others 4 phases are constituted by the campaign and the analysis of the data acquired during the 3 campaigns 2013, 2014, 2015 and 2016 . Phase-1 of the activity was devoted to the preparation of an improved version of the L-band microwave radiometer RADOMEX as well as the definition of acquisition procedure and campaign execution. Phase-1 started in January 2012 and ended in October 2012, the performed activities were reported in the CIP and RR document of the contract [3][4][5].

Phase-2 of the activity, is constituted by the deployment of the instrument during the first summer Antarctic campaign 2012, the acquisition of the data during 2013 and its analysis and the preparation for the Austral summer campaign 2013. It started in November 2012 and ended in October 2013. Results are presented in the First Year Report of the project [6].

Phase-3 of the activity is the subject of this document, it includes the execution of the Antarctic summer campaign 2013 and the acquisition and analysis of the data were collected from December 2013 to December 2014.

The different sections of the document describe the execution of the summer campaign 2013 and the activities were conducted in Antarctica and in Italy during the austral winter. A significant activity was carried out in this period is the theoretical interpretation of observed Tb data. This is described in detail in the document. The data acquisition and analysis (D3) is contained here, the collection of the photographic material is contained in the D4 of the project and the data are contained in D5.

3 The 2013 Summer Antarctic Campaign

The second Antarctic campaign of the project (hereinafter referred as Domex-3) was funded by the PNRA in the framework of the Monitoring Antarctic Ice Sheet using Advanced Remote Sensing Systems - MAISARS project. This latter aims at investigating on the structure and the properties of the snowpack at Concordia Station by means of several different remote sensing sensors and to inter-compare their results.

The aim of the 2013 Antarctic campaign of the project concerned the maintenance of the instruments already deployed on the field by IFAC-CNR during the 2012 expedition. Also, a secondary topic of the campaign was the search for potential RFI which could affect the microwave brightness temperature measurements. In the following sections the work carried out on the field will be detailed described. For this second campaign the team was composed by Marco Brogioni of IFAC.

3.1 Description of the campaign

The summer campaign of MAISARS started on November, 9th 2013 when Marco Brogioni reached Concordia Station (he departed on November 2nd from Italy). Three main activities were performed during the campaign:

- realignment of the snow temperature probes buried in the snowpack and maintenance of their datalogger,
- maintenance of Radomex instrument; in detail: substitution of the Radomex loads reference power supply, improvement of the heater system inside of the instrument box and in the external enclosures where the actuators are located,
- search for radio frequencies interferences (RFI) which occasionally affect the brightness temperature measurements.

The first week in Concordia Station (Nov, 11th – 17th) was characterized by a cold and windy weather which makes almost impossible the logistic operations. The activities during this week were focused on a revision of the data collected in the past year, on the improvement of the procedure used to transmit data to Italy, and on performing an inventory of the spare parts of Radomex already present in the base. On Nov, 14th the weather get slightly better and the operations on the snow temperature datalogger started. The first one was the dig of a trench in the snow in order to recover all the probes buried in the first meter. Once the probes were found they were put at the same depth (approx. 50cm deep) and left in place until the following Sunday for intercalibration purposes. After this operation the power cable of the datalogger was substituted with one made in silicon rubber because the shelter was not heated anymore because of the energy reduction policies of Concordia Station recently adopted. The new cable ensures the proper functionality of the datalogger even in case of very low temperature. Then, on Sunday 17th the snow temperature probes were put at the nominal depth (Fig.1) and the snow trench buried.

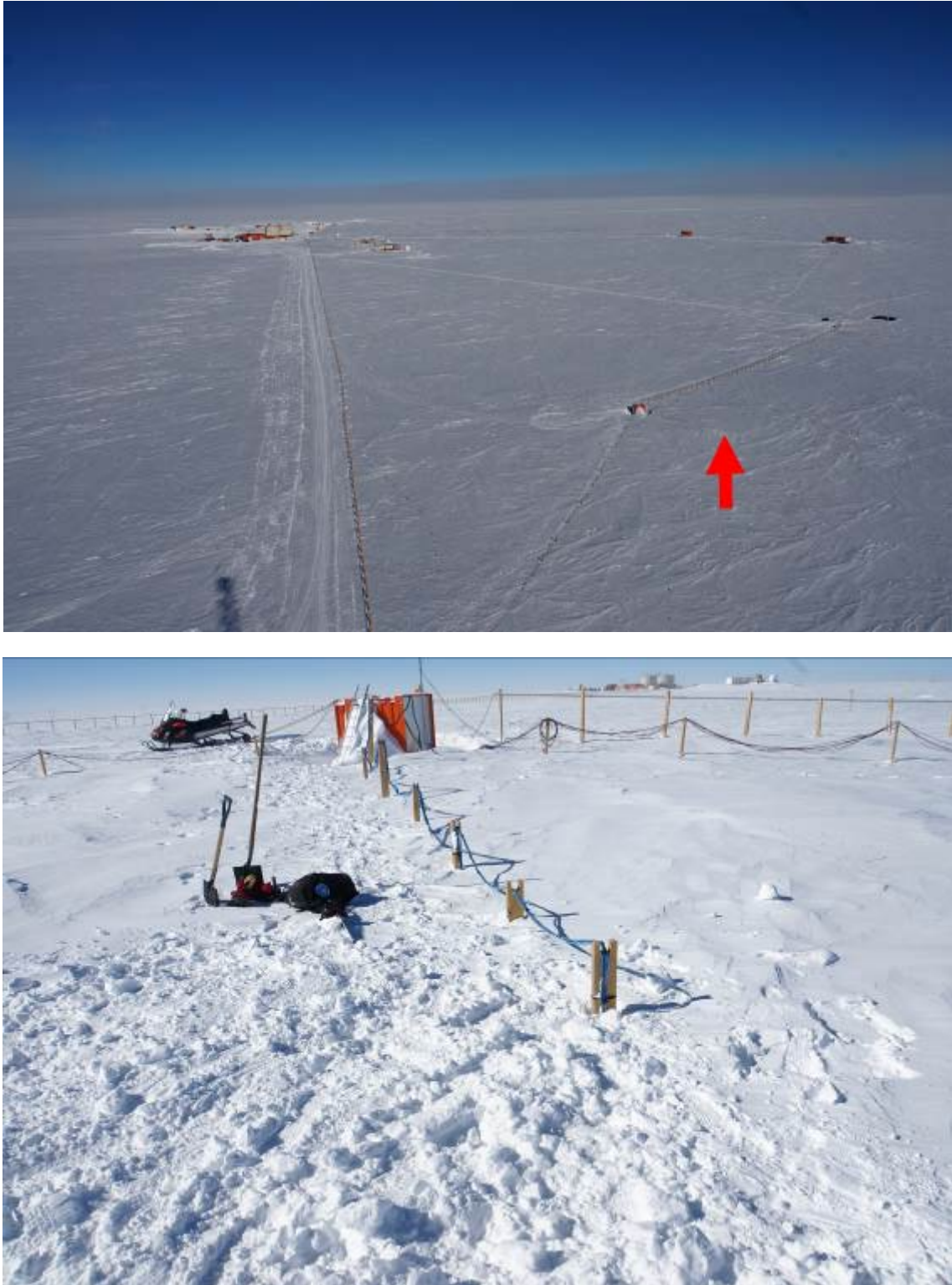


Figure 1. Location of the snow temperature probes as seen from the US tower (top) and from ground after the maintenance (bottom). Red arrow in the top image indicates the exact location of the probes.



Figure 2. The snow pit in which are located the snow temperature probes (left) after the re-alignment to their nominal depth. The image on the right shows a particular of the probes.

On Monday 18th, after an improvement of weather condition, the radiometer was removed from the US tower and stored in the Free-Time Tent, which is the only location devoted to science with enough space for operating on the instrument. The first activity on Radomex was performed on the RF receiver in order to substitute a 12V power supply which underwent to a failure during the 2013 austral winter. At the same time the PT100 transmitters of the internal calibration system (hot and cold loads at 250°C and 340°C respectively) were replaced with ones which have a broader measurement range (100°C instead of 50°C). This operation was done to avoid any potential problem in case of another power supply failure. After these substitutions the receiver returned in fully operating conditions and was tested by connecting the inputs of the receiver to two matched loads instead of the antenna outputs.

While the RF receiver was under testing, the thermal system of Radomex was improved with more efficient components and the whole instrument underwent to an accurate inspection in order to detect any possible problem **Figure 3**. On Saturday 22nd all the tests on the Radomex subsystems were passed thus the instrument was re-assembled. On Monday 25th the instrument was placed outside of the tent for a check in real operative conditions, Fig.2. Since Radomex performances complied with the nominal ones, the instruments was deployed on the US tower on Nov 28th and put in calibration mode by observing alternatively the deep sky and the snowpack. On Dec, 2nd a noise was detected in the Radomex measurements. After having performed a further set of test, the cause of the problem was found in the not proper functioning of the V polarization antenna RF connector. On December 6th the problem was fixed and Radomex returned to its proper functionality. Instruments was then tested over different targets in order to check its proper functioning. In particular clear sky, and matched loads were observed from December 4 to December 7. Unclaibrated Tb values of this period are represented in **Figure 5**.

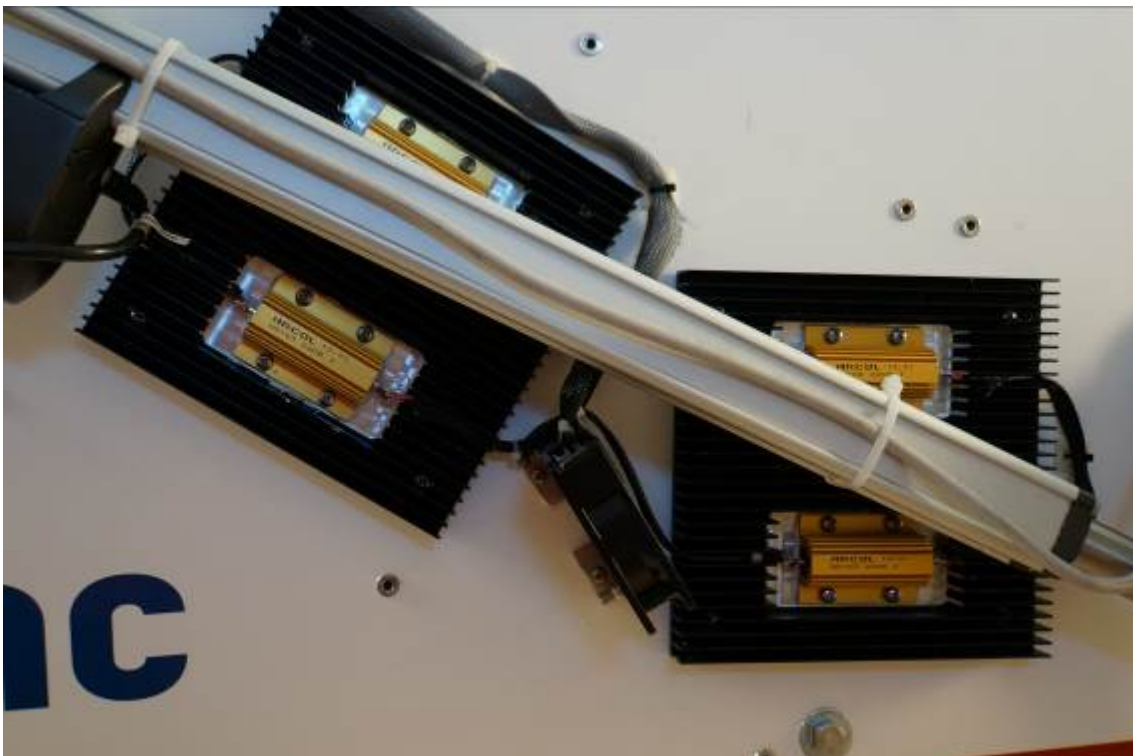


Figure 3. The heaters installed on the roof (top) and inside the external carters (bottom) of the Radomex enclosure. In order to diminish the stress of the thermal system, five new heaters were added on the roof (the smaller ones) and the value of the shielded resistances in the carters halved.



Figure 4. Radomex re-assembled during the functionality test outside the free-time tent (before the deployment on the tower).

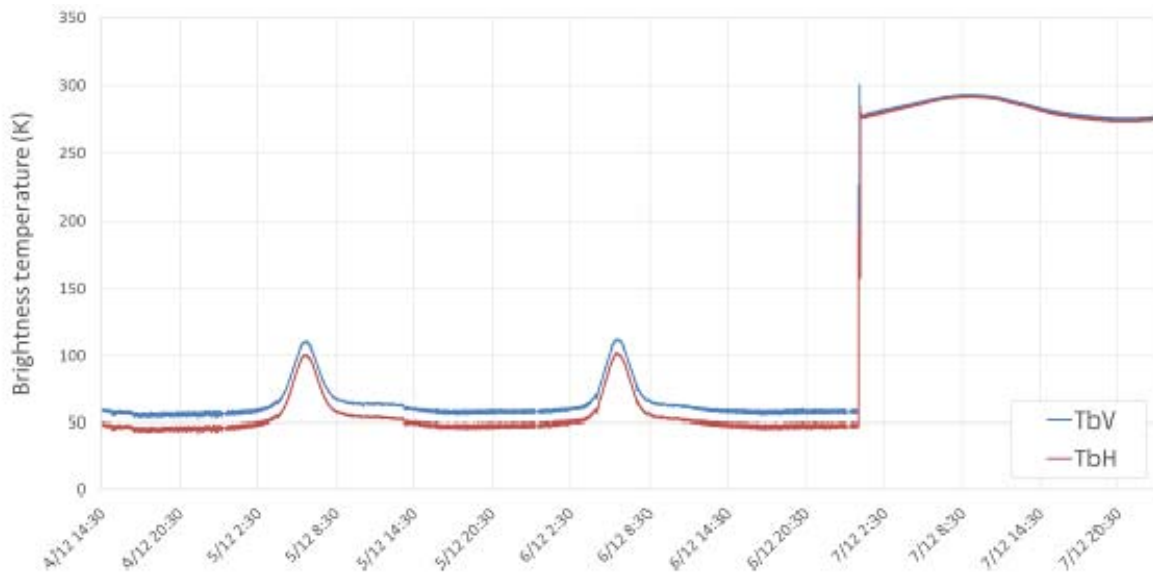


Figure 5. Sky and matched load measurements performed before the departure from the base.

In the meanwhile, the search for radio-frequency interference which affected the microwave L-band measurements in the previous year was performed. It is worth to remind that the frequency range 1400-1427 MHz is a protected band in which any kind of artificial electromagnetic emission is forbidden according (e.g. ITU-R Recommendation RS.2017). RFI were searched from the free time tent, from the base and from the US tower shelter towards the main experiments and buildings, allowing a complete scan of all the possible sources even coming outside of the base (see Figure 6):

- From the summer camp towards the base (1)
- From the base towards Superdarn experiment (2)
- From the base towards Fisica, Sismo and Glacio shelters (3)
- From the US tower towards the base and summer camp (4)
- From the US tower towards Fisica, Sismo and Glacio shelters (5)
- From the US tower towards Superdarn experiment(6)

In two cases, an unexpected emission at 1440 MHz with an intensity around -70 dBm was detected (even if not recorded) from the free-time tent when observing in direction of the base and the tower (approx. North-West). Unfortunately, it was not possible to individuate the source of the emission due to the short duration of the signal.

The campaign ended on Dec, 8th when Marco Brogioni left Concordia Station onboard of the Twin Otter; he arrived in Italy on Dec. 24th.

3.2 Activity with the winterover researchers

In order to allowing the proper continuation of the Domex-3 experiment and its related activities Paride Legovini (the engineer in charge of the scientific experiments during the 2014 winterover) was trained in order to operate on Radomex (both on the software and on the device) and on the snow temperature datalogger. The snow conventional measurements were in charge of Igor Petenko who had already spent a winterover at Concordia Station in the past. In particular, the measurements he carried out were:

- daily precipitation particles and fresh snow (daily);
- snow accumulation (weekly);
- superficial snow density: 8 samples at 10 cm below the surface in the surroundings of the snow poles for the seasonal accumulation estimation (bi-weekly)
- first meter snow density at 10 cm steps (monthly).



Figure 6. Location and directions of the RFI measurements (top) and measurement setup below the US tower (bottom).

4 2014 Winter Period

The winter period concerns the period for December 2013 (when CNR people left the base) to December 2014. Main activities were carried out in Antarctica and area related to radiometer acquisition while some activities were conducted in Italy. Both of them are briefly described in the following subsections. Data analysis and processing is contained in section 5 of the document-

4.1 Radiometer acquisition

RADOMEX acquired data all over the year from December 2013 to December 2014. In general data were acquired at the nominal fixed incidence angle of 42° 24h/24h whereas in some occasion angular scans and sky observation were performed.

During the whole period the instrument acquired data regularly with any special problem although some power failure of the tower power system determined a sequence of switching on and switching off of the whole system which determines the loose of the data for some periods. Moreover it was observed that, both in summer and winter, after the switching off the quality of the data deteriorate and it needs a certain time to recover. The time depends on the duration of the switching off and the temperature reached by the system. Over a total number of 392 days the acquisition was performed on 362 days corresponding to 91% of the period.

Figure 7 represents a summary of the acquisition. In figure 1 represents acquired data while 0 no data. The duration of the interruptions is, in general, for 1 or 2 days. The longer interruption, 15 days, occurred in September 2014.

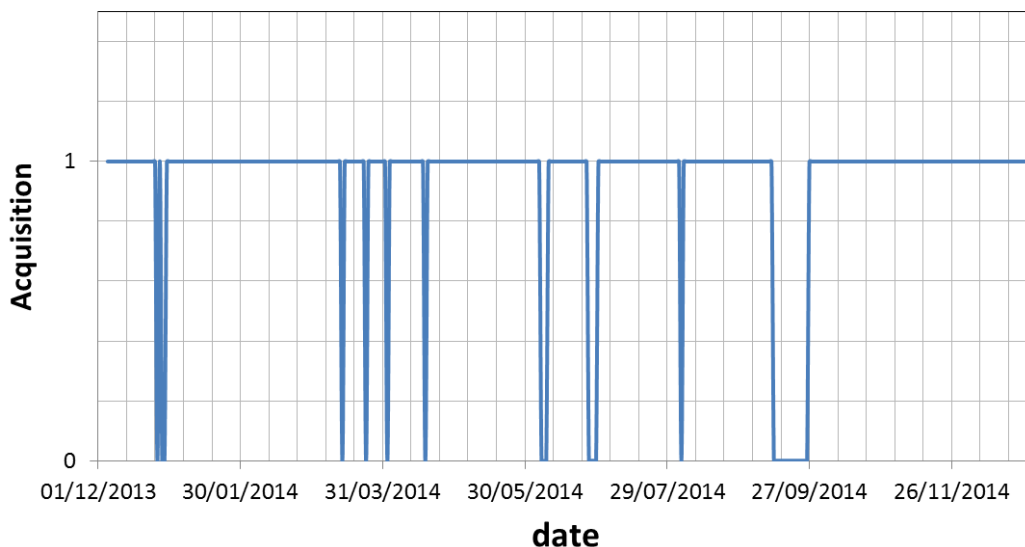


Figure 7. Summary of the acquisition: 1 represents acquired data while 0 no data.

Concerning the acquisition mode it is worth to notice that up to august 2014 the radiometer operated in normal mode using the standard calibration scheme which is based on the measurements of two reference loads having two different temperatures.

Nevertheless some anomalies were recorded in the data starting from April 2014. The number of anomalies increased in time up to beginning August. By an in depth analysis of the data it was observed that the anomalies were due to a malfunctioning of the cold load which leads to an error in the computation of the gain and offset of the system and finally to errors in the computed T_b . Detail and adopted correction for that period are in depth described in the following section.

After several attempts and interactions between the IFAC team and the winterovering personnel it was decided to configure the system in a different operation mode and using the reference noise as second calibration load. The procedure and the concept was in depth described in a previous report [6] and not repeated here.

Using this configuration data were acquired for the rest of the period. As noticed during the first year of the campaign the only problem we registered is that data are intrinsically low stables in the short time period since the T_n is not timely stable as the T_c . This means that the typical T_b standard deviation was around 0.1 K over a period of 1 minutes for the typical radiometer configuration (2 loads) and around 0.5 K for the new one.

The radiometer was re-configured in August 8 and continuously operated in this mode until the end of the winter campaign.

Tests and check were performed along the campaign in order to verify the calibration of the system including sky observations and incidence angle scans.

4.2 Snow activities

During winter period the outdoor activities are strongly limited by the extreme environmental conditions. Main activity concerns the verification of the snow temperature acquisition system. Data were automatically registered on the datalogger and, one per month, transferred to the base and the in Italy.

Snow density in the first meter was also measured during the whole season. Data were collected one per month.

4.3 2014 Activity at IFAC

The main activity was conducted at IFAC was the data analysis and processing which is described in section 5. Moreover other activities were necessary for the preparation and activation of winter campaign 2014 were carried out in that period.

4.3.1 Preparation of material for 2014 summer campaign

Considering the problems that affected Radomex during the 2014 winter, an activity was carried out to prepare a second receiver can be used as spare part in case of need during the campaign.

The second receiver, which was already available at IFAC, was in depth characterized and calibrated.

As an example in **Figure 8** is represented the comparison between the measured brightness temperature and the physical temperature of the matched load inserted in a thermal bath and which was connected to the receiver inputs.

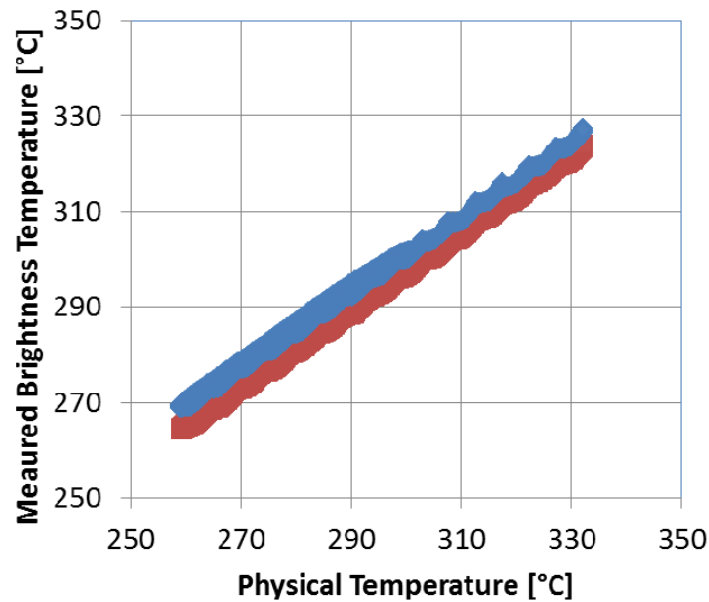


Figure 8. Measured Brightness Temperature and Physical Temperature

Red and blue color represents the two different receiver ports respectively. Data demonstrate the linearity of the receiver in the observed range.

Figure 9 represents a test of the temporal stability of the receiver. Data on a stable target (matched load) were acquired for a period of 300 minutes. The physical temperature is very stable showing a standard deviation less than 0.01 °C, the brightness temperature is also stable exhibiting a standard deviation of around 0.1 K.

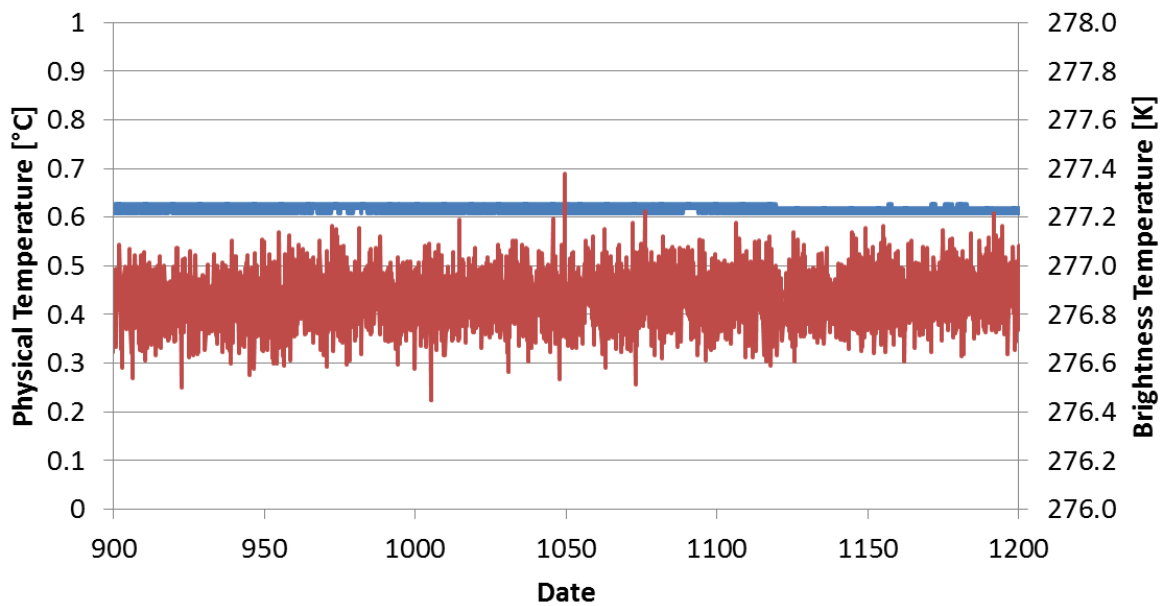


Figure 9. Measured Brightness Temperature and Physical Temperature

The receiver was also characterized as losses of the different components (cables, etc.) and prepared for Antarctic shipment.

4.3.2 Preparation for the 2014 summer campaign

The experimental campaigns at Concordia Station can be carried out only after the authorization of the experiment from PNRA (or IPEV for the French researchers). In order to get the approval, IFAC have to submit a project in the framework of the PNRA calls. This approval is necessary to perform the experiment but also guaranteed the shipment of the materials to and from Dome C, all the expenses related to the personnel while abroad, the organization and realization of the entire journey, the training of the researchers for operating in the Antarctic environment, the availability of a researcher during the austral winter which will continue the experimental activities, the availability of all the facilities on-site.

The first year of experimental campaign was carried out at Concordia Station in the framework of the PNRA project MAPME 2009/A3.05 which ended in 2013. In order to prosecute the Domex-3 experiment a new project called MAISARS 2013/AC3.07 was submitted to PNRA in March 2013 and received the approval in August 2013. The new project guaranteed the entire execution of the Domex-3 campaign 2014.

Following the expected plan, it was then expected that a new summer campaign was scheduled for 2014 year. Nevertheless, because of some problem occurred in the logistic organization of the campaign (PNRA-IPEV) it was decided, in agreement to the Agency, that the participation of people directly involved in the DOMEX project was not necessary.

Indeed in July 2014, when the campaign was planned, it was pointed out that that, due to a lack of fuel replenishment during the previous years (caused by anomalous sea ice around the coast which prevent the

arrival of the French ship), most of the effort of the Italian-French Agency during the summer campaign were devoted on the re-fueling of the Antarctic stations. For this reason, any new scientific activity was possible for 2014. Because the MAISARS project, led by IFAC, involved other experiments that cannot be executed in this campaign, and the number of campaigns per project is limited, we decided to postpone the experiments by one year. On the other hand, results obtained during 2014 demonstrated that instrument's performances were within the requirements in term of temporal stability and accuracy and we retained that an intervention on RADOMEX was not needed.

Moreover, a special attention was devoted to the training of the 2015 winterover personnel (Dr. Giampietro Casasanta) which spent some days at IFAC.

4.3.3 Theoretical Modelling of DOMEX data

An important activity was carried out during the second year of the project was the modelling and explanation of the L-band brightness temperature signature of the Antarctic plateau. Indeed, although for the Dome C area the steadiness of the brightness temperature at V polarization is assessed, H polarization shows some variations which are not completely understood. Moreover, since Domex-1 experiment there was the evidence that the emission of the Antarctic plateau differs from other regions of the Earth due to the strong layering and the thickness of the ice which made possible to avoid the influence of the underlying ground. In particular the V polarization angular trend showed a dynamic much higher than expected and the polarizations difference resulted to be greater than what predicted by model simulations performed until the first experiment. Thus an accurate modeling of the Tb signature is fundamental to explain all the features observed in the Domex Tb timeseries.

In order to investigate the physical reasons which led to the particular microwave emission of the East Antarctic Plateau, appreciable efforts have been put in coupling an advanced electromagnetic model with ground measurements and geophysical models. In particular the influence of natural snowpack variability on L- and C- band microwave emission have been explored. The work was carried out in cooperation with Prof. Kenneth (prof. emeritus at the Byrd Polar Research Center - Ohio, USA) who contributed to the glaciological aspects of the study.

Datasets used

Two data-sets obtained at different frequencies were used: C-band data were acquired during the pilot-experiment DOMEX-1 in December 2004 and L-band angular scan data collected during the DOMEX-2 and DOMEX-3 experiments. The use of two wavelength is very important because they have different penetration depth and carry information about different part of the ice sheet (the top 50-100m for the C-band and ~500m for the L-band).

C-band data

For comparing the measured Tb data to model simulations a sub-sample of measurements collected during a period of one week from December 25 to December 31 at a fixed azimuth angle of 0° (i.e. the same was used for the L-band acquisitions) was selected. The Tb value at each incidence angle (in the range 25°-75° at 5° step) was computed as the average value of the measurements collected in this period. For each angle the standard deviation was also computed and ranged from around 1 K at 25° of incidence angle to around 3 K at 70° of incidence angle. This relatively large value is due to the daily fluctuation of Tb as mentioned above. Near-surface, snow-temperature profiles, were collected in the same period and were used as inputs for model simulations.

L-band data-set

Regarding the L-band angular scan, all the data collected during DOMEX-2 and DOMEX-3 experiments were averaged with the exception of data collected when the sun is in front of the antenna. A total of around 4000 scans was considered. For each angle (from 20° to 60° at 10° steps) the Tb standard deviation was between 0.4 K and 0.7 K and between 1.3 K and 3.2 K at V and H polarization respectively. Snow

temperature profiles of the upper 10 meters collected simultaneously with the electromagnetic measurements were averaged and the average used as input to the electromagnetic model.

Microwave modeling

The model used to simulate the Tb was the Dense Medium Radiative Transfer theory under the Quasi-Crystalline Approximation with Coherent Potential – DMRT-QCACP (Tsang et al., 2001) in the multilayer version (DMRT-ML) implemented at LGGE (Picard et al., 2013). DMRT-QCACP simulates the scattering of the spherical particles under the Rayleigh approximation. Given the wavelengths involved (21.2 cm at L-band and 4.4 cm at C-band) with respect to the mm scale dimensions of the snow crystals, the applicability of this approximation was met.

The model represents the snowpack as a stack of layers with flat interfaces above a semi-infinite medium either representing ice, soil or water. Each layer is characterized by its temperature, thickness, snow density and grain radius. Ice permittivity is obtained by means of (Tiuri et al., 1984) while water dielectric constant can be found in (Meissner and Wentz, 2004). As indicated in (Picard et al., 2013) the emission of the snowpack was simulated by considering ice spheres embedded in air for layers in which the density was less than the half of the pure ice density (i.e. 461 kg/m³) and as air spheres in ice for a density above that threshold. Air bubble dimensions were obtained from (Ueltzhoffer et al., 2010).

The firn physical properties needed for simulating the brightness temperature of the snowpack were obtained both from in situ data and from the literature. Near surface in situ measurements were conducted within the framework of DOMEX experiments. Data from previous ground campaigns located in the same area were also used (e.g. (Urbini et al., 2008)). Layering, density, temperature and grain radius were obtained in the upper 10 m from the several snow pits dug on the test site during DOMEX experiments described in (Macelloni et al., 2006) and (Macelloni et al., 2013). Below 10 meters the needed input parameters were obtained by using snow glaciological models constrained by the experimental measurements with the exception of the density measurements from 10 to 50 m obtained from (Urbini et al., 2008). The vertical profiles for each snow parameter used in the simulations are described in the following.

Snow temperature profile

The snow temperature profile was obtained by merging together the data collected at Concordia Station (Macelloni et al., 2006) in the upper 10 m in order to account for the seasonal temperature swing, and the formula in (Jesek et al., 2015) for the snow layers deeper than 10 m. In fact, as shown in (Macelloni et al., 2013), the snowpack seasonal temperature variability decreases as the depth increases and is less than 0.3 °C at 10 m deep. Thus it can be ignored for model simulations.

The snow temperature expressed as a function of depth (z) is:

$T(z < 10m, t) = \text{Experimental data}$

$$T(z \geq 10m) = T_m - \frac{G \sqrt{\pi}}{2 k_c \sqrt{\frac{M-m}{2 k_d H}}} \left[\operatorname{erf} \left(z \sqrt{\frac{M-m}{2 k_d H}} \right) - \operatorname{erf} \left(H \sqrt{\frac{M-m}{2 k_d H}} \right) \right] \quad (1)$$

where T_m is the mean annual surface temperature (which was measured to be 218.2 K for Dome-C area), M is the mean accumulation rate (18.2 mm yr⁻¹), m is the basal melting rate (0.0007 mm yr⁻¹), H is the ice thickness (3200 m), k_c is the ice conductivity (2.7 W m⁻¹ K⁻¹), k_d is the ice diffusivity (45 m² yr⁻¹), and G is the geothermal heat flux (0.0533 mW m⁻²). All the above parameters were derived from (Bereiter et al., 2014) with the exception of T_m which was obtained from the measurements. As described previously, the experimental data in (1) are the average values of the ground measurements collected during the whole T_b measurement period at each frequency considered (one week for the C-band, three years for the L-band). Figure 10 represents the temperature profile used for simulating C-band data. In the upper-right box of the figure the temperature of the first 20 meters is also represented. It can be observed that the temperature decreases from the surface to 5 meters deep because data were collected during the summer season. Data were well in line with (Bereiter et al., 2014).

Snowpack density profile

Ground measurements showed that the vertical snow density profile increases with depth with a superimposed, spatially-varying fluctuating part (Macelloni et al., 2013). Moreover, measurements showed that the density fluctuations are higher near to the surface and tend to disappear as a function of depth (Hörhold et al., 2011). The average vertical profile used in this work was obtained from (Bingham and Drinkwater, 2004) for coarse grains

$$\rho(z) = 0.922 - 0.573 e^{-0.0163z} \quad (2)$$

As presented in Figure 11, the model (2) agrees on average with data collected during ground experiments at Dome-C reported in (Ueltzhoffer et al., 2010) and (Hörhold et al., 2011). The same model predicts a close-off depth (i.e. the region below which the air is trapped and isolated completely from outside atmosphere as defined in (Aranud et al., 2000) at around 115 m deep where the density reaches a value of 0.83 g/cm³ and the value of 0.922 g/cm³ at a depth of 300 meters.

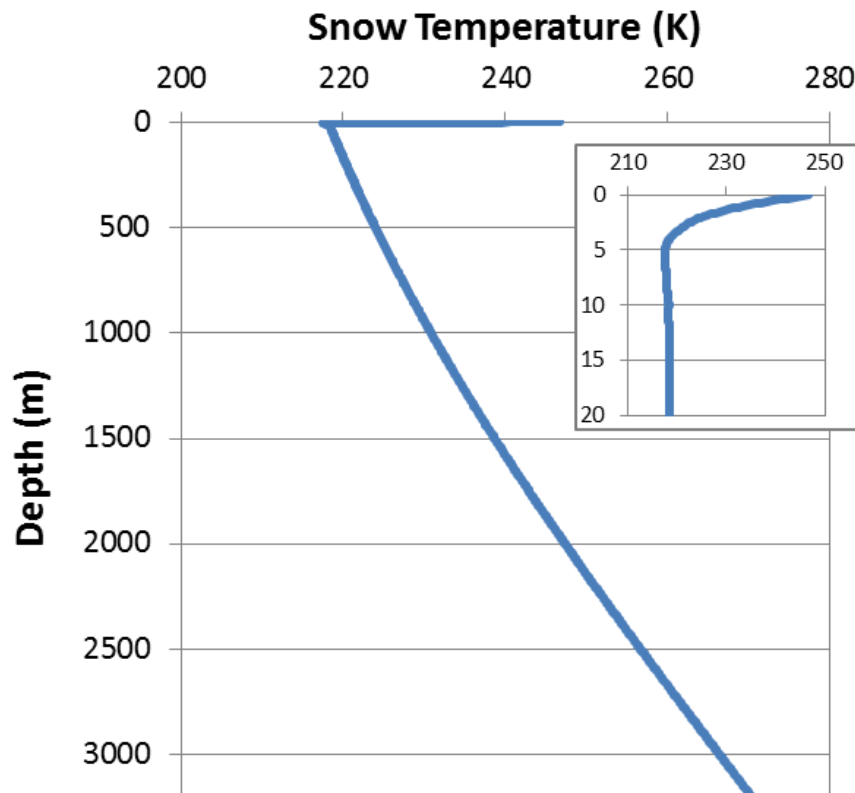


Figure 10 – Snow temperature profile as obtained by equation (1). The inset on the right represents the temperature of the first 20 m for the last week of 2004 (when the 6.8GHz Tb was collected).

While available data are useful for the computation of the average density trends, they are not sufficient for a rigorous computation of the fluctuating part. Indeed whereas a certain number of density measurements are available in the first 5 m (around 70 profiles mostly concentrated in the upper 2 meters), only a reduced number are available for 5 to 10 meters (6 profiles) and only very few for deeper layers (and in any case limited to the upper 50 m). Moreover, field measurements demonstrated that, for the fluctuating part, the snow density profile is spatially inhomogeneous at a few meters scale (Picard et al., 2014).

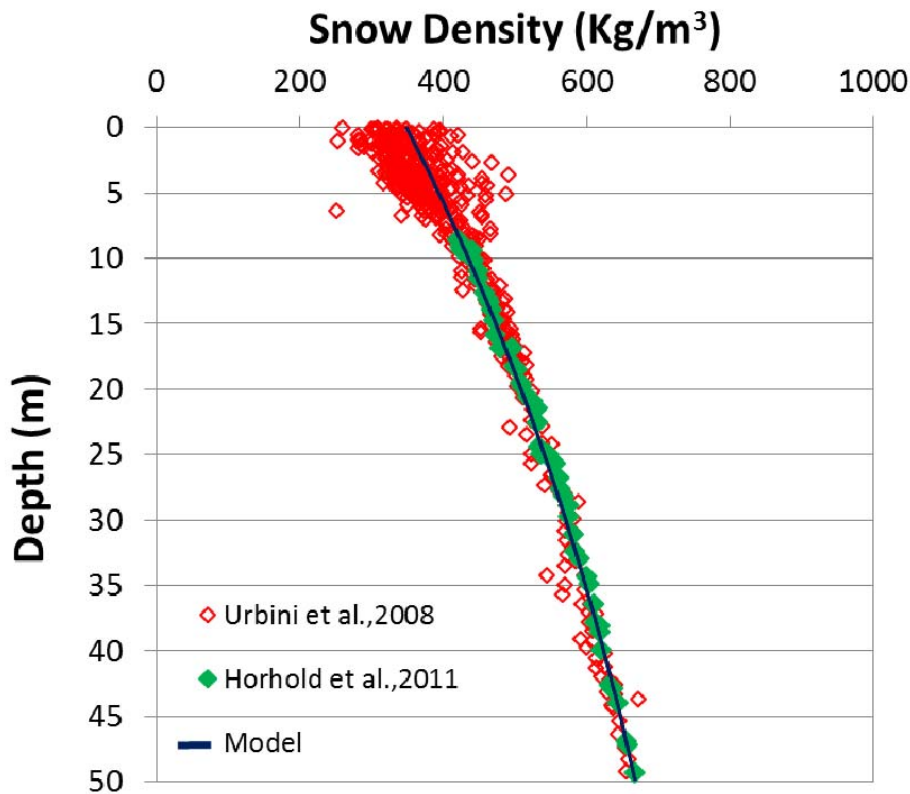


Figure 11 – Snow density profile in the upper 50 meters measured in the area of Dome C ((Macelloni et al., 2006), (Macelloni et al., 2013) and (Urbini et al., 2008) red diamonds; (Horhold et al., 2011) green diamonds; model (2) blue line).

As an example, Figure 12 represents three density profiles collected at the same time in the upper 100 cm at a separation distance of about 2 meters each. We observe that although the values are always between 300 and 400 kg/m³ they differ considerably at each depth as a function of the location where the pit was dug. Data collected in others pits, as well as data published in (Horhold et al., 2011) Urbini et al., 2011) collected in the same area, lead to a similar conclusion. (Horhold et al., 2011) also pointed out that the density variation decreases as a function depth until it reaches a minimum of 6 kg/m³ when the mean density value is around 600 kg/m³.

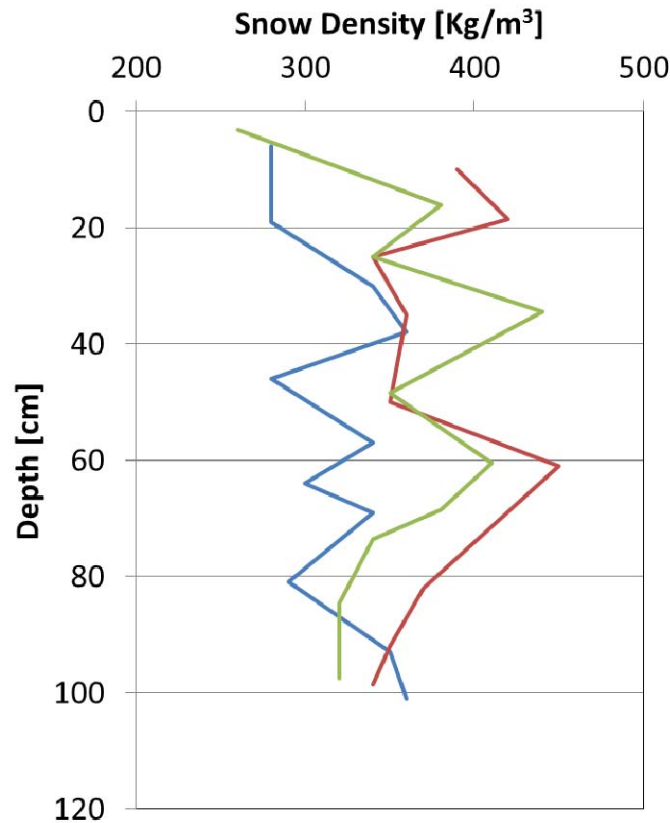


Figure 12 – Snow density profiles in the upper meter measured over about 4 to 5 meters of distance. Measurements were collected at different depths depending on snow layering (Picard et al., 2014).

As input to the radiometric model, the density fluctuations were added to the average vertical profile by means of Gaussian damped noises as suggested in (West et al., 1996)

$$\tilde{\rho}(z) = \rho(z) + N(\sigma_{\rho}) e^{-z/\alpha_{\rho}} + N(\sigma_{\rho d}) \tag{3}$$

For a layer at depth z , the model density profile (3) is composed of a mean value $\rho(z)$, a Gaussian noise $N(\sigma_{\rho})$ with a standard deviation σ_{ρ} times an exponential term (α_{ρ} is the vertical damping factor) which accounts for muting the density variation as the firn compresses to ice plus a term $N(\sigma_{\rho d})$ which accounts for the fluctuation of deep layers (i.e. from 600 to 922 kg/m³). In our case we use a $\sigma_{\rho d}$ value of 6 kg/m³ according to (Horhold et al., 2011).

Snow pits in the upper 1-5 m show that the standard deviation of the density measurements (i.e. density measured at the same depth but in different places) is on the order of 45-55 kg/m³ and also that density fluctuations were poorly correlated layer to layer. Because equation (3) presents two unknowns (σ_{ρ} and α_{ρ}) in this study, several values of σ_{ρ} and α_{ρ} , in the range 40-60 kg/m³ and 10-35 m respectively were considered. Because the density fluctuations were modeled as a stochastic process, a Monte Carlo analysis

was performed for determining the average emission of the snowpack. Specifically for each couple of $\sigma\rho$ and $\alpha\rho$ a number of realizations were performed and the T_b is computed as the average of the realizations.

As pointed out previously, ground measurements show that there is a certain degree of vertical correlation (although small) between the density of the snow layers, however the data collected were not sufficient to determine the correlation function accurately. In order to account for this phenomenon, we considered two different cases for the realization of the noise stochastic process. In the first case, the noise realizations are independent layer by layer. In the second case, we assume an exponential correlation as suggested in (Tsang and Kong, 2001) with a correlation length of 10 cm. The former case was intended to represent correlations at short scale while the latter was selected for correlations at longer scale. The 10 cm value corresponds to the average thickness of the layers in the top part of the snowpack (as observed in the ground measurements collected in the first 5 meters). The correlation between layers tends to further damp the layer to layer density variability without which the layer densities change in an unnaturally abrupt way.

Figure 13 provides an example of a complete density profile used for the model simulation. In this case 60 kg/m³ and 35 m were used for $\sigma\rho$ and $\alpha\rho$ respectively. The density of the upper 50 meters is also shown as an inset.

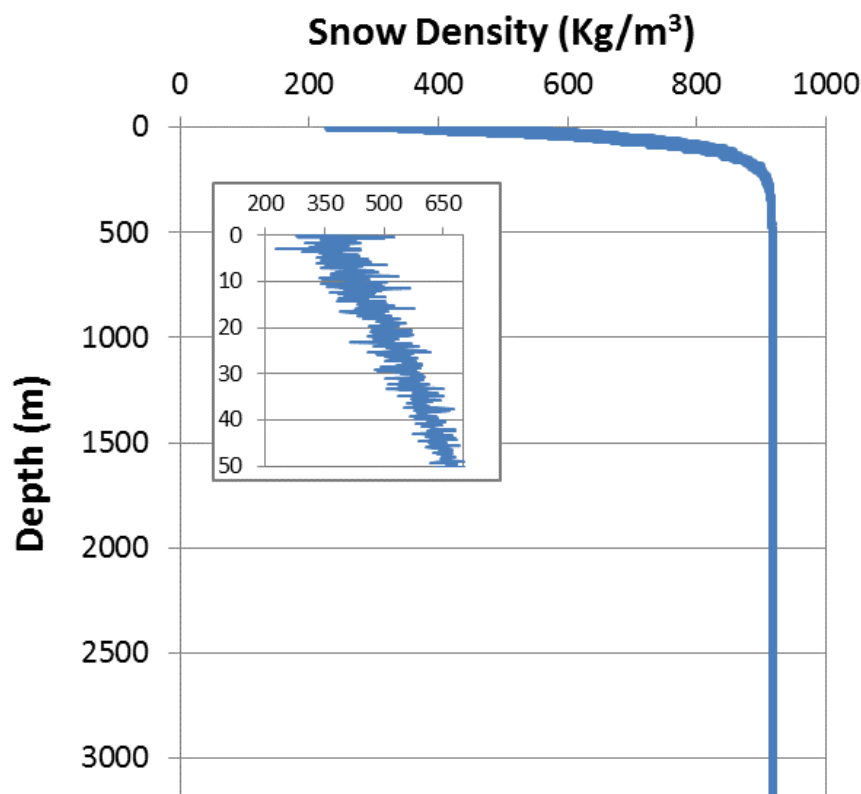


Figure 13 – Example realization of snow density obtained by choosing $(\sigma\rho, \alpha\rho) = (60 \text{ kg/m}^3, 35 \text{ m})$. Density in the upper 50 m is highlighted in the inset.

Snowpack grain radius profile

DMRT-ML models the snowpack as a stack of layers composed of spherical particles and requires as input the vertical profile of the sphere scatterers radius. Because the shape of the real snow crystal is relatively different from the spherical one, a common approach is to input the model with a scaled version of the real ground measurements (Tedesco et al., 2006)

The grain radius continuous profile $a(z)$ considered in the present task was the one published in (Zwally H., 1977) adjusted to fit the Tb measurements at L- and C- band

$$a(z) = k \sqrt[3]{0.0377 + 0.00472z} \quad (4)$$

where k is the fitting parameter which will be determined, as discussed in the following section, by fitting Tb data at V polarizations close to the Brewster angle.

As with the density profile, conventional grain size measurements (i.e. according to (Fierz et al., 2009) performed during DOMEX and SSA (Specific Surface Area) measurements presented in (Gallet et al., 2011) show that the grain size profile is spatially variable. An example of the variability of grain size dimensions as a function of depth and space collected during DOMEX is presented in Figure 14. Measurements in the figure represents the maximum dimensions of prevailing grains (in mm) observed in the same pits of Figure 12.

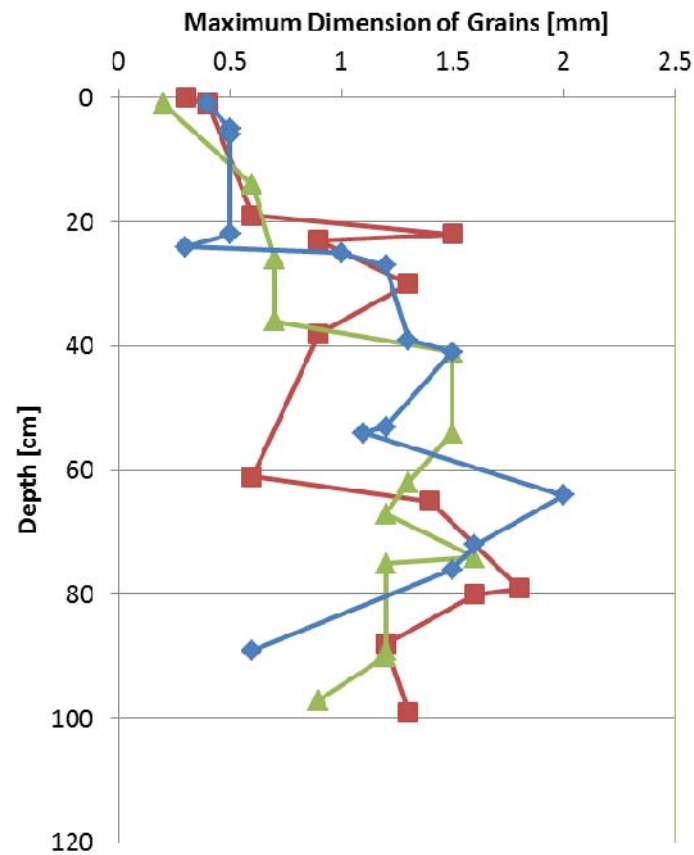


Figure 14 – Maximum dimension of prevailing grains in the first meter measured in three different snow pits at about 5 meters of total separation. Measurements were collected at different depths depending on snow layering (Picard et al., 2014).

Also in order to describe the grain size fluctuation we use a function similar to that used for the density profile:

$$\tilde{a}(z) = a(z) + N(\sigma_a) e^{-z/\alpha_a} \tag{5}$$

In this case five values for σ_a were considered, from 0 (no noise added) up to 0.3 mm in step of 0.1 mm, and four values for α_a , i.e. 25m, 50m, 75m and not damped.

Because at L- and C-band the scattering of the ice crystals is very small due to the size of the scatterers with respect to the wavelengths involved in the study (tenths of mm with respect to several cm) it is expected that the influence of grain size fluctuations is negligible at L-band but could be appreciable at C-band.

Layering profile

As pointed out in (Macelloni et al., 2006), (Macelloni et al., 2013), (Gallet et al., 2011) and (Groot Zwaaftink et al., 2013) the layer thickness of the snowpack at Dome C is not homogeneous. Dominant layers associated with annual variations in surface density and accumulation rate will thin with depth due to firn compaction. At Dome C, and based on a simple mass continuity model (West et al., 1996), a layer at the surface will thin by about a factor of 2 once it reaches a depth of about 100 m. In order to represent this effect, and to limit the total number of layers in the electromagnetic model to reduce the computations time, we considered a fine sampling of the top part of the snowpack, in which the snow properties changes are appreciable (i.e. temperature, density and grain size), and a more coarse sampling of the deeper parts in which the firn have already reached the close-off condition. To model the layer thickness in the first 50 meters (i.e. the depth where the density fluctuations reach the minimum as shown before) we use the approach of (Herron and Langway, 1980). By using the mean density profile and a constant surface accumulation rate the mass continuity can be expressed as

$$h(j) \rho(j) = h(j+1) \rho(j+1) \quad (6)$$

where $(h(j), \rho(j))$ and $(h(j+1), \rho(j+1))$ are the thickness and density of two successive layers. $h(0)$ was assumed to be equal to one year's worth of accumulation which, for Dome-C area is about 0.1 m/yr ((Petit et al., 1082), (Frezzotti et al., 2005)). By using equation (2) and (6) it is possible to obtain iteratively the layers thickness. After 50 m a coarser layer sampling was used. Table 1 summarizes the layer scheme used for model simulations. Ground measurements carried out in the Dome-C area highlighted a high spatial variability of the layering in the area (Picard et al., 2014). For representing the thickness variability we added a Gaussian uncorrelated noise with zero mean to the layering profile. Thus the depth of the layer interfaces can be expressed by

$$\tilde{d}(z) = d(z) + N(\sigma_d) \quad (7)$$

The standard deviation σ_d was set to the 15% of the layer thickness and the absolute value of $N(\sigma_d)$ limited to $3\sigma_d$. An example of layers thickness distribution obtained from such procedure is represented in

Figure 15.

In order to speed up the computations, in the case of C-band simulations the number of layers has been limited to the first 300 m because penetration depth at this frequency is on the order of tens of meters (Macelloni et al., 2007).

Table 1 – Layers scheme used in model simulations

Depth	N. of Layers and Thickness
0-50	According to the model (6)
50 -100	500 layers, 10 cm each
100 to 300m	400 layers 50 cm each
300 to 3200	480 layers 6 m each

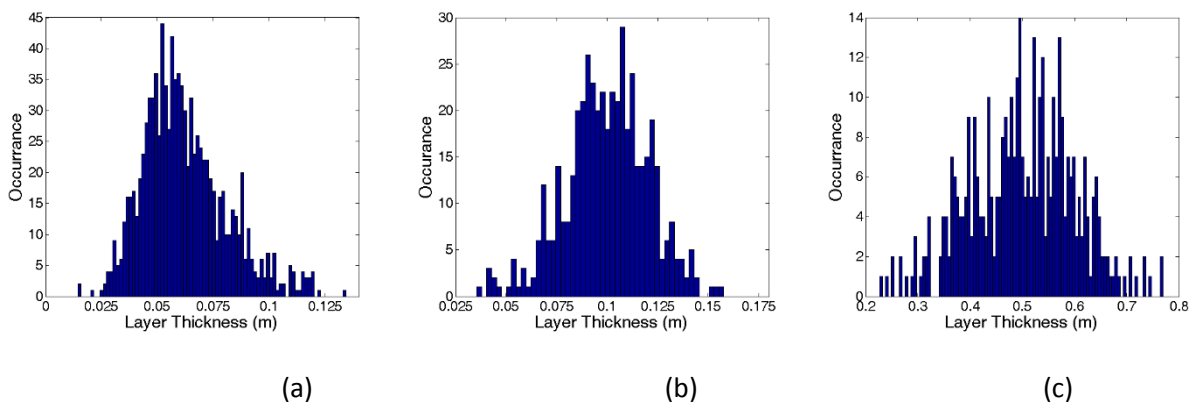


Figure 15– Histograms of layer thickness in the depth range 0-50m (a) (layer thickness is variable), in the depth range 0-100 m (layers thickness 10 cm (b)) and in the depth range 100-300m (c) (layer thickness 50 cm). Data from one realization of the stochastic process are represented here.

In addition to depth varying properties of the firn and ice, we need to select the properties of the ice sheet base. At the bottom of the ice sheet, we assume a film of water above rock as suggested in (Carter et al., 2009) and (Zirizzotti et al., 2012).

Electromagnetic Model Results

The first step of the modeling is to determine the grain radius fitting parameter k . The k parameter was selected as the value that minimized the difference between measured and simulated T_b at C- and L-band for data collected at 60° , which is close at the Brewster angle, and V polarization. For this configuration the electromagnetic emission is minimally influenced by the layering (i.e. by the surface scattering) and it is

possible to use, as model inputs, the density, grain size and layering parameters obtained from regular monotonic profiles disregarding their fluctuations. The analysis reveals that the k parameter is important at C-band and negligible at L-band. As k changes from 2 to 5, T_b decreases by about 40 K at C-band and 0.1 K at L-band. The best k value is 3.7 which is in line with previous studies (Picard et al., 2013). For this value the T_b difference between data and model is 0.3 K and 2.5 K at C- and L-band respectively.

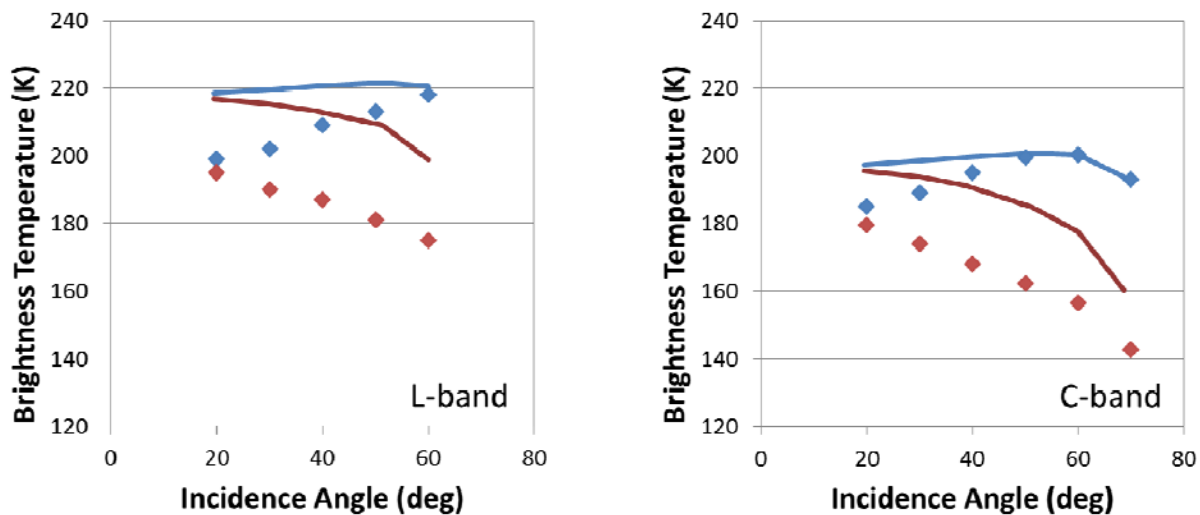


Figure 16 - Brightness temperature at L-band (left) and C-band (right) as a function of the incidence angle. Experimental (dots) and model data (lines) are represented in blue for the V pol and red for the H one. Simulated T_b are obtained by considering continuous snow parameters profiles.

The comparison between model and measured data as a function of incidence angle at both frequencies, polarizations and for all the incidence angles using the so obtained k value is presented in Figure 16.

Figure 16 clearly demonstrates that at V polarization the model and data agree at the angle where the minimization procedure was performed but disagree at all the other angles at L-band and at angles lower than 50° at C-band. H-polarization is always overestimated by about 20 K at both frequencies. Moreover the difference between V and H polarizations is not reproduced. As expected, the result points out that as expected, the assumption of a smooth density function is insufficient to model the whole angular range. Indeed, assuming a continuous density profile, the permittivity of two overlapped layers is almost the same, the scattering at the interfaces between the layers is not accounted for properly, and the resulting surface scattering is negligible. On the other hand, because of the relatively long wavelength with respect to the grains size dimension volume scattering is less important and so cannot adjust the model to fit the data over the whole incidence angle range. This result, also obtained in (Tsang and Kong, 2001) and (Leduc-Leballeur, 2015), suggests the introduction of fluctuations in the density profile are particularly important in the case of the Antarctic firn, due of the number of layers (i.e. more than 700 layers in the first 50 meters) that composed the snowpack combined with the high penetration depth of electromagnetic waves at low-microwave frequencies (Macelloni et al., 2007).

Once the k factor was set, the first step of the Monte Carlo analysis to include layers was to determine the minimum number of realizations that should be produced for each kind of stochastic variability in density, grain size and layering in order to have a sufficient statistics. For each parameter ($\sigma\rho$ and $\alpha\rho$ for density, $\sigma\alpha$ and $\alpha\alpha$ for grain size, σd for layering) we considered several cases and 500 realizations were produced for each one. By averaging more than 100 realizations the mean values of the Tb became stable with a maximum variation of 0.3 K (i.e. lower than the accuracy of the DOMEX data as discussed in section 2) between 50 and 100 realizations. The following analyses were conducted by considering 100 realizations of the stochastic processes. Figure 17 shows the mean Tb values at V and H polarization at 40° of incidence angle as a function of the number of realizations for which the mean value of the realizations was computed. In this case all the input noise parameters of the profile were kept constant and the density profile was characterized by the pair $(\sigma\rho, \alpha\rho) = (60 \text{ kg/m}^3, 35 \text{ m})$.

The Monte Carlo study continued with modifications to the stochastic density parameters. This was done to simultaneously minimize the difference between measured and simulated Tb angular variations at V and H polarizations for the L- and C-band data. Figure 18 shows the simulations results obtained for the most extreme cases considered at L-band.

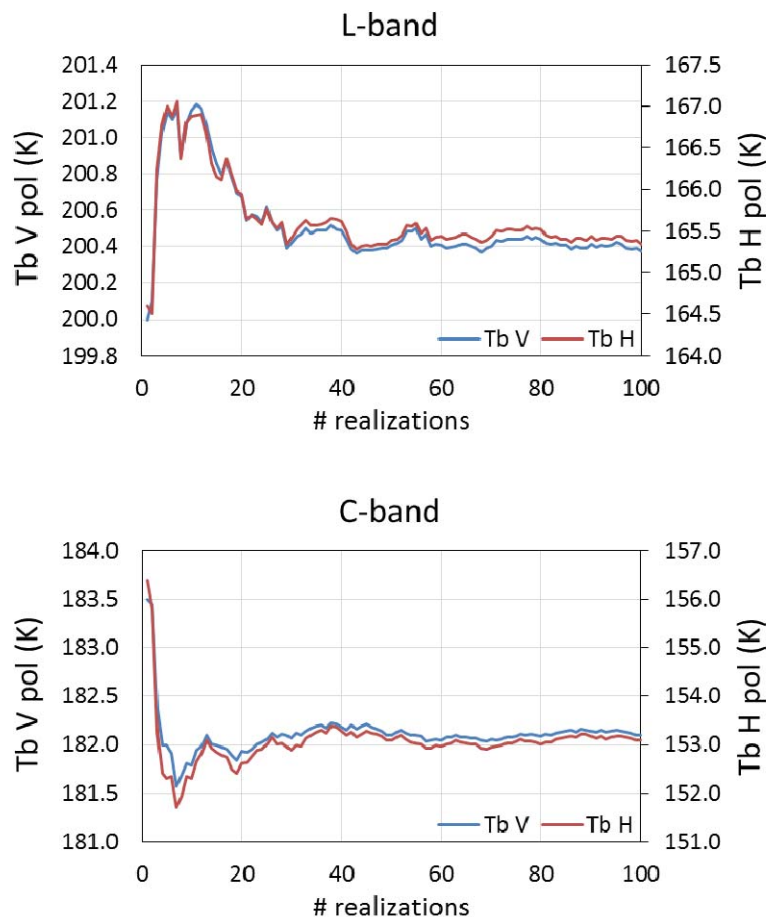


Figure 17- Simulated Tb at L- and C-band as a function of the number of the realizations considered in the Tb average (incidence angle 40 deg). V polarization is represented in blue and H pol in red. Here the model was run with a noise density profile characterized by the pair $(\sigma\rho, \alpha\rho) = (60 \text{ kg/m}^3, 35 \text{ m})$.

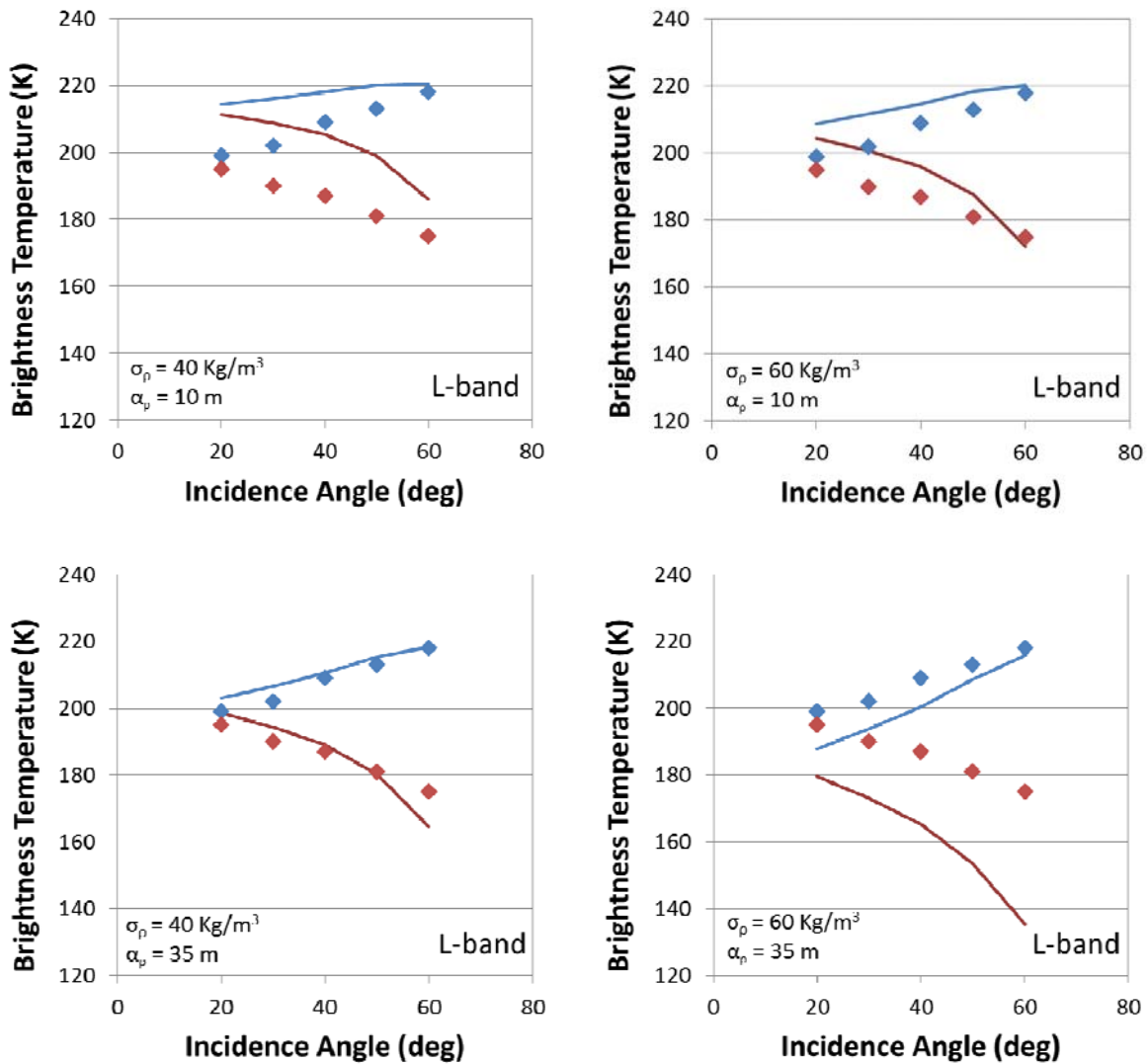


Figure 18 – Comparison between DOMEX Tb measurements (dots) and DMRT-ML simulations (lines) by considering a fluctuating density profile. The model was run by considering the most extreme values for (σ_ρ , α_ρ): left column shows simulations with $\sigma_\rho = 40 \text{ kg/m}^3$, right column with $\sigma_\rho = 60 \text{ kg/m}^3$, top row results were obtained with $\alpha_\rho = 10\text{m}$ while bottom row with $\alpha_\rho = 35\text{m}$. V and H polarizations are represented in blue and red respectively.

As expected, by increasing σ_ρ (the magnitude of the density fluctuations) and/or α_ρ (the depth at which the fluctuations are reduced by $1/e$) Tb decreases because the surface scattering at the interfaces becomes stronger. Also, the introduction of the density fluctuations makes it possible to better reproduce the experimental Tb trends, absolute values, and polarization differences. Note that Tb at V polarization at angles close to the Brewster remains almost constant as assumed in the grain radius fitting procedure.

By computing the Root Mean Square Error (RMSE) between experimental and model datasets for all the combinations of $\sigma\rho$ and $\alpha\rho$ it was possible to find the values which are best able to reproduce the DOMEX data.

Figure 19 presents maps of RMSE values for V and H polarizations at L- and C-band as a function of $\sigma\rho$ (horizontal axes) and $\alpha\rho$ (vertical reversed axes) for uncorrelated (top) and correlated (bottom) density fluctuations. For this simulation a correlation length of 10 cm was used. Also the RMSE obtained by considering both polarizations together ("V + H" case) is depicted. The black dashed lines, included for reference, indicate the range of the density standard deviation computed from ground measurements collected about Dome C. Figure 19 shows that there is a belt of pairs $(\sigma\rho, \alpha\rho)$ which give the same RMSE value. Moreover, figure 10 shows that the RMSE features obtained by considering correlated fluctuations of density are shifted towards higher standard deviation values. This was quite expected because the assumption of correlated density variations implies that on average the densities of overlapping layers are more similar than in the uncorrelated case. In turn, there is less surface scattering which reflects in a higher RMSE error for a given $(\sigma\rho, \alpha\rho)$ pair.

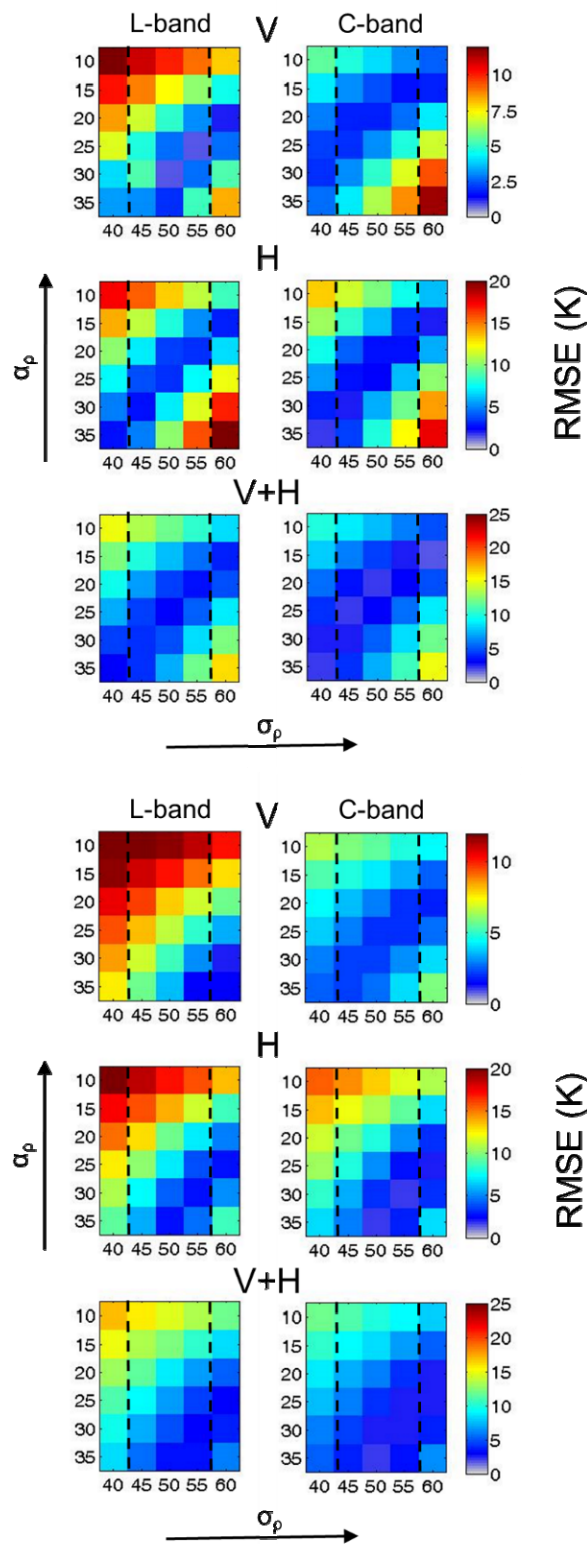


Figure 19- RMSE images computed at V polarization (top row), H polarization (medium row), “V and H” polarizations at L- and C-band as a function of σ_ρ (horizontal axes) and α_ρ (vertical reversed axes) for uncorrelated (left) and correlated (right) density fluctuations. Black dashed lines indicate the standard deviation range of the density measurements collected on ground at Dome C.

The analysis of the RMSE obtained by considering the different kinds of stochastic processes (i.e. uncorrelated and correlated) indicates that for the uncorrelated noise the lowest RMSE values are reached when the $\sigma\rho$ is in the range measured in situ at Dome C. The minimum RMSE value is obtained for the pairs $(\sigma\rho, \alpha\rho) = (55 \text{ kg/m}^3, 20 \text{ m})$ for the uncorrelated case and $(55 \text{ kg/m}^3, 30 \text{ m})$ for the correlated one. In order to verify that these results are representative of real data we compare density realizations obtained with these two pairs to the available ground data as reported in (Ueltzhoffer et al., 2010) (Hörhold et al., 2011) and (Picard et al., 2014). As an example Figure 20 shows the density variability as a function of mean density as measured at Dome-C ((Ueltzhoffer et al., 2010) (Hörhold et al., 2011)) and obtained with the pairs which provides the best T_b for the uncorrelated case. Figure 11 demonstrates that modeled density variability as a function of density is in agreement with measurements. The differences between ground and modeled data are due both to the reduced number of ground data and the simplified representation of the ice sheet used in the electromagnetic model.

After investigating the sensitivity of brightness temperature to the density variations, the study focused on the influence of grain radius profile fluctuations on the T_b . Only the best uncorrelated case of density profile was considered for this analysis.

As described in the previous section, the perturbations added to the grain radius profile had a standard deviation σa which varies from 0 mm (no noise added) up to 0.3 mm in step of 0.1 mm, and a αa damping factor of 25 m, 50 m, 75 m and not damped. The tails of the Gaussian distribution were limited to a minimum grain radius of 0.1 mm. Results of the analysis are shown in Figure 21.

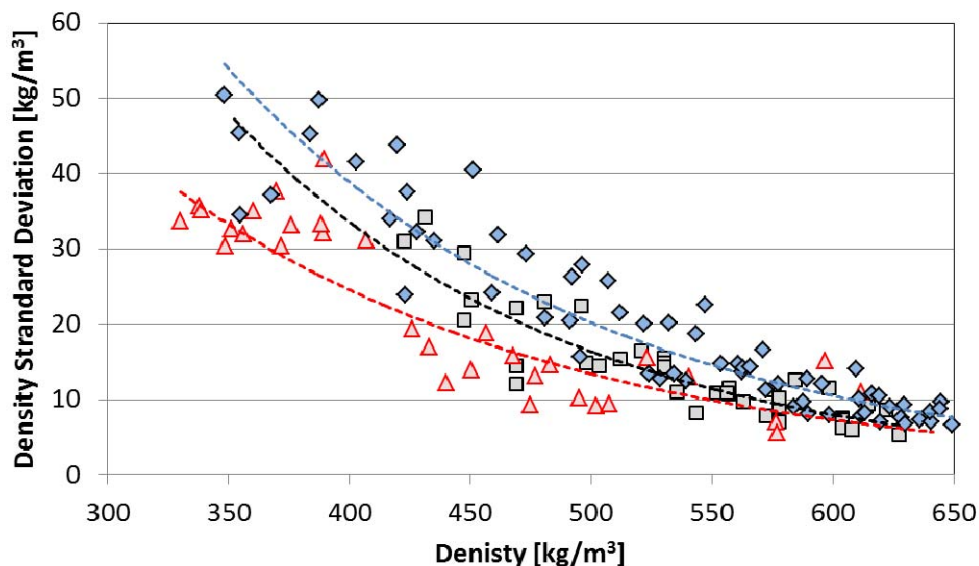


Figure 20- Density variability as a function of mean density: Red triangles and grey squares are obtained from (Ueltzhoffer et al., 2010) and (Hörhold et al., 2011). Blue diamond represent an example of a profile obtained using the pairs $(\sigma\rho, \alpha\rho) = (55 \text{ kg/m}^3, 20 \text{ m})$ for the uncorrelated case. Dashed lines represent the interpolant of the data.

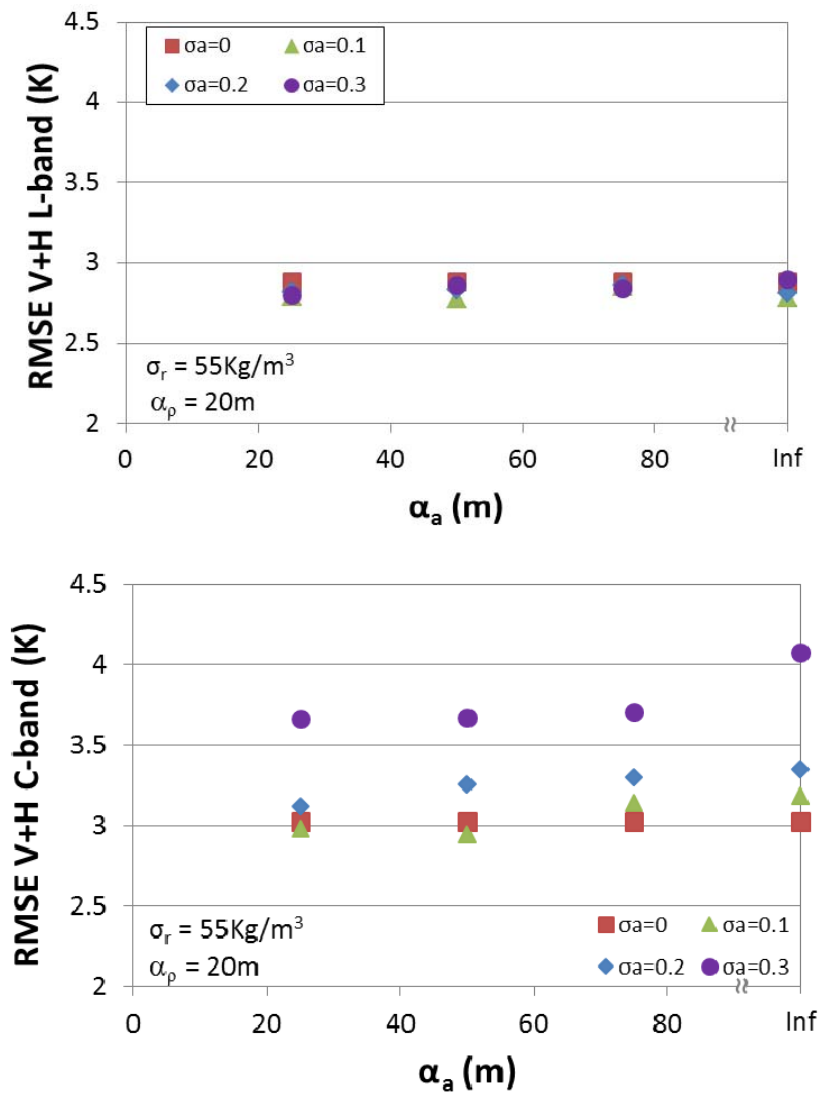


Figure 21 – Global RMSE (V+H pols) computed for $\sigma_r = 55 \text{ kg/m}^3$ and $\alpha_p = 20 \text{ m}$ as a function of the grain radius damping factor α_a for four values of σ_a . Simulations at L- (top) and C-band (bottom).

At L-band, the random fluctuations of the grain radius profile do not affect the brightness temperature. This result was quite expected because at 1.4 GHz the wavelength is at least two order of magnitude greater than the size of the scatterers. At C-band, the influence of the grain size is also weak and is appreciable only for σ_a values higher than 0.2 mm. Indeed the increasing of the standard deviation σ_a above 0.2 mm leads to an increase of 0.5 K of the RMSE values. The damping factor α_p have a certain effect only for its highest values.

The last point of the study was devoted to analyze the influence of the layering fluctuations on T_b . The simulations revealed that the microwave emission at both L- and C-band is quite insensitive to the fluctuations in the layer thickness (the T_b variations are of the order of few tenth of K). This indicates that, using an incoherent model, the surface scattering at the several layer interfaces (depending on real part of

firn permittivity fluctuations which are in turn linked to density) are more relevant than the layer extinction (which depends on layer thickness and ice losses).

By analyzing the results of all the cases considered, best fitting is obtained for an uncorrelated noise on the snow density characterized by the pair $(\sigma\rho, \alpha\rho)=(55 \text{ kg/m}^3, 20 \text{ m})$ and grain radius by $(\sigma a, \alpha a)=(0.1 \text{ mm}, 50 \text{ m})$ (Figure 22). The RMSE values at L- and C-band are 3 K and 2 K respectively. The disagreement between simulated and measured H pol data at L-band at high incidence angle could be explained by the fact that the interfaces between the snow layers (considered flat and horizontal in this work) could have a small roughness w.r.t. the wavelength and could not be perfectly horizontal.

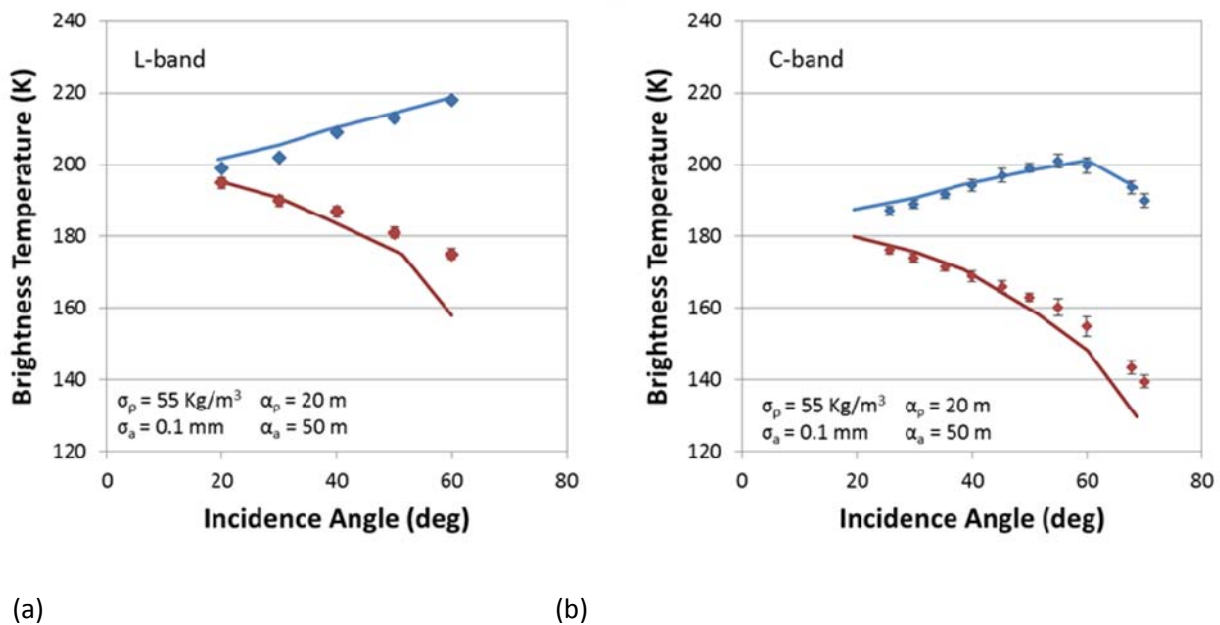


Figure 22- Brightness temperature at L-band (a) and C-band (b) as a function of the incidence angle at V (blue) and H (red) polarizations. Experimental (dots) and model (continuous lines) data produced by using a density and grain radius fluctuating profiles with $(\sigma\rho, \alpha\rho)=(55 \text{ kg/m}^3, 20 \text{ m})$ and $(\sigma a, \alpha a)=(0.1 \text{ mm}, 50 \text{ m})$ respectively.

An additional test has been conducted on the impact of the grain size fitting parameter k which was selected at the beginning of the analysis. Using the pairs of Figure 22

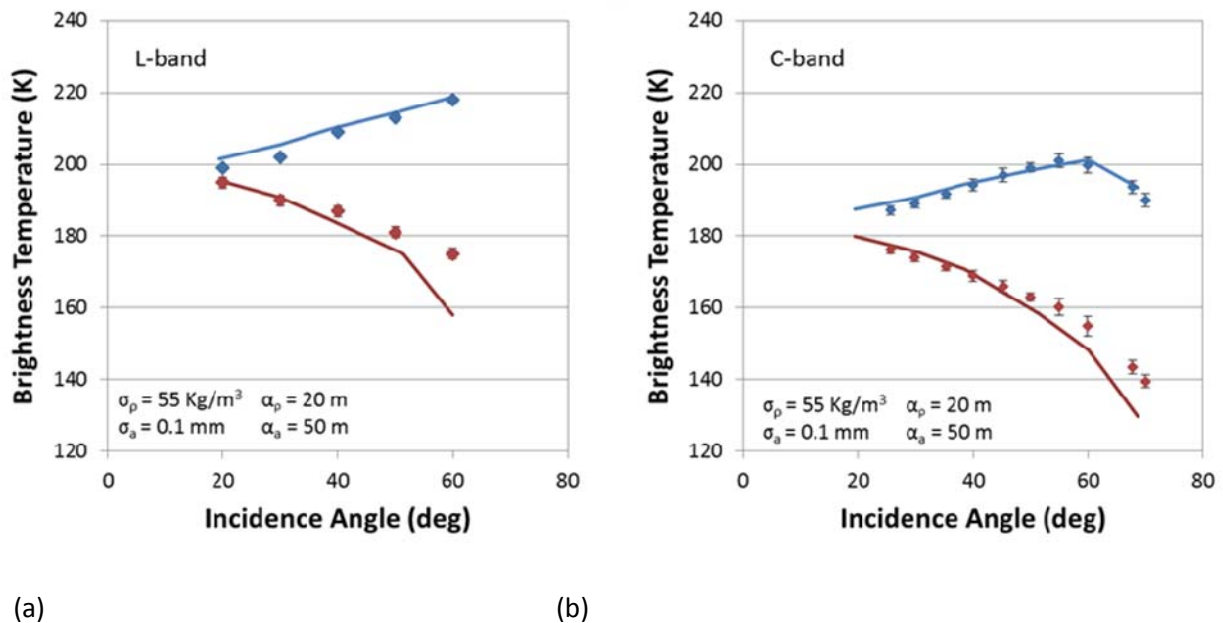


Figure 22, model simulations were performed for $k = 3$ and $k = 5$. As expected, the effect on the L-band is negligible while at C-band the results are worst and the RMSE is 8.6 K and 25.7 K for $k = 3$ and $k = 5$ respectively.

Remarks

This activity permitted to explain clearly the microwave emission mechanisms which take place at Dome C. Also it serve as a basis to analyze all the variations which can be found in the Domex timeseries. Due to its wide frequency range, this study allows the synergistic use of different sensors operating in the low microwave frequency spectrum like AMSR2 or Windsat.

The study has been accepted for publication on the Microrad 2014 Special Issue of IEEE JSTAR journal. The reference is

Brogioni, M.; Macelloni, G.; Montomoli, F.; Jezek, K.C., "Simulating Multifrequency Ground-Based Radiometric Measurements at Dome C—Antarctica," Selected Topics in Applied Earth Observations and Remote Sensing, IEEE Journal of , vol.PP, no.99, pp.1,13, doi: 10.1109/JSTARS.2015.2427512

References (only valid for this section)

Arnaud L., J.M. Barnola and P. Duval, "Physical modeling of the densification of snow/firn and ice in the upper part of polar ice sheets". In: Hondoh T, ed. Physics of Ice Core Records. Sapporo: Hokkaido University Press, pp. 285—305 , 2000

Bereiter B., H. Fischer, J. Schwander, B. Stauffer and T.F. Stocker, "Diffusive equilibration of N2, O2 and CO2 mixing ratios in a 1.5 Million Years Old Ice Core", The Cryosphere, 8, 245–256, 2014

Bingham A.W. and M. R. Drinkwater, "Recent Changes in the Microwave Scattering Properties of the Antarctic Ice Sheet", IEEE Trans. On Geoscience and Remote Sensing, Vol.38, no.4, pp. 1810 - 1820, Jul 2000

Carter P., D. D. Blankenship, D. A. Young, and J. W. Holt, "Using radar- sounding data to identify the distribution and sources of subglacial water: Application to Dome C, East Antarctica," J. Glaciol. , vol. 55, no. 194, pp. 1025–1040, Dec. 2009;

Fierz, C., Armstrong, R.L., Durand, Y., Etchevers, P., Greene, E., McClung, D.M., Nishimura, K., Satyawali, P.K. and Sokratov, S.A. 2009. The International Classification for Seasonal Snow on the Ground. IHP-VII Technical Documents in Hydrology No. 83, UNESCO-IHP, Paris. 90 pp

Frezzotti M. et al. , "Spatial and temporal variability of snow accumulation in East Antarctica from traverse data," J. Glaciol., vol. 51, no. 172, pp. 113–124, 2005

Gallet, J.C., F. Domine, L. Arnaud, G. Picard and J. Savarino, "Vertical profile of the specific surface area and density of the snow at Dome C and on a transect to Dumont D'Urville, Antarctica – albedo calculations and comparison to remote sensing products", Cryosphere, vol. 5(3), pp. 631–649, 2011.

Groot Zwaafink C.D., A. Cagnati, A. Crepez, C. Fierz, G. Macelloni, M. Valt and M. Lehning, "Event-driven deposition of snow on the Antarctic Plateau: Analyzing field measurements with SNOWPACK", Cryosphere, vol. 7, pp. 333-347, 2013

Herron, M.M. and C.C. Langway, Jr. 1980. Firn densification: an empirical model J. Glaciol.,25 (93), 373–385

Hörhold M.W., S. Kipfstuhl, F. Wilhelms, J. Freitag and A. Frenzel , "The densification of layered polar firn" J. Geophys. Res. Vol. 116, 2011

Jezek K.C., J.T. Johnson, M.T. Drinkwater, G. Macelloni, L. Tsang, M. Aksoy and M. Durand, "Radiometric Approach for Estimating Relative Changes in Intraglacier Average Temperature", IEEE Trans. on Geoscience and Remote Sensing, vol.53, no.1, pp.134,143, Jan. 2015

Leduc-Leballeur, M.; Picard, G.; Mialon, A.; Arnaud, L.; Lefebvre, E.; Possenti, P.; Kerr, Y., "Modeling L-Band Brightness Temperature at Dome C in Antarctica and Comparison With SMOS Observations," Geoscience and Remote Sensing, IEEE Transactions on , vol.PP, no.99, pp.1,11 doi: 10.1109/TGRS.2015.2388790

Macelloni G., P.Pampaloni, M.Brogioni, A.Cagnati, M.Drinkwater, "DOMEX 2004: an experimental campaign at Dome-C Antarctica for the calibration of space-borne low-frequency microwave radiometers", IEEE Trans. On Geoscience and Remote Sensing, Vol.44, no.10, pp. 2642 - 2653, Oct. 2006

Macelloni G., M. Brogioni, P. Pampaloni and A. Cagnati, "Multi-frequency Microwave Emission from the East Antarctic Plateau: Temporal and Spatial Variability", IEEE Trans. Geosci. Remote Sensing (Microrad 08, Special Issue), vol. 43, pp.2029-2039, July 2007

Macelloni G., M. Brogioni, S. Pettinato, R. Zasso, A. Crepez, J. Zaccaria, B. Padovan, M. Drinkwater, "Ground-Based L-Band Emission Measurements at Dome-C Antarctica: The DOMEX-2 Experiment", IEEE Trans. On Geoscience and Remote Sensing, Vol.51, n.9, pp. 4718 - 4730, Sep. 2013

Meissner T. and F. Wentz, "The Complex Dielectric Constant of Pure and Sea Water from Microwave Satellite Observations", *IEEE Trans. On Geoscience and Remote Sensing*, Vol.42, no.9, pp. 1836 - 1849, Sep 2004

Petit J., J. Jouzel, M. Pourchet, and L. Merlivat, "A detailed study of snow accumulation and stable isotope content in Dome C (Antarctica)," *J. Geophys. Res.-Oc.*, vol. 87, no. C6, pp. 4301–4308, 1982.

Picard G., L. Brucker, A. Roy, F. Dupont, M. Fily, and A. Royer, "Simulation of the microwave emission of multi-layered snowpacks using the dense media radiative transfer theory: the DMRT-ML model", *Geoscientific Model Development*, vol. 6, pp. 1061-1078, 2013

Picard, G., Royer, A., Arnaud, L., and Fily, M.: Influence of meter-scale wind-formed features on the variability of the microwave brightness temperature around Dome C in Antarctica, *The Cryosphere*, 8, 1105-1119, doi:10.5194/tc-8-1105-2014, 2014.

Tedesco M., E.J. Kim, D. Cline, T. Graf, T. Koike, R. Armstrong, M. J. Brodzik and J. Hardy, "Comparison of local scale measured and modelled brightness temperatures and snow parameters from the CLPX 2003 by means of a dense medium radiative transfer theory model", *Hydrol. Process*. Vol. 20, pp. 657–672, 2006

Tiuri M., A. Shivola, E.G. Nyfors and M.T. Hallikainen, "The Complex Dielectric Constant of Snow at Microwave Frequencies", *IEEE Journal of Oceanic Engineering*, Vol. 9, No. 5, pp. 377-382, December 1984

Tsang, L. and J.A. Kong, *Scattering of Electromagnetic Waves*, vol. 3, Advanced Topics, Wiley Intersci. and Hoboken, N. J., 2001

Ueltzhoffer K.J., J. Kai, V. Bendel, J. Freitag, S. Kipfstuhl, D. Wagenbach, S.H. Faria and C.S. Garbe, "Distribution of air bubbles in the EDML and EDC (Antarctica) ice cores, using a new method of automatic image analysis", *J. Glaciol.*, Vol. 56 n. 196, pp. 339–348, 1020

Urbini S., M. Frezzotti, S. Gandolfi, C. Vincent, C. Scarchilli, L. Vittuari and M. Fily, "Historical behaviour of Dome C and Talos Dome (East Antarctica) as investigated by snow accumulation and ice velocity measurements", *Global And Planetary Change*, Vol. 60, n.3-4, pp. 576–588, Feb 2008

West R., D. Winebrenner, L. Tsang and H. Rott, "Microwave Emission From Density-Stratified Antarctic Firn At 6 Cm Wavelength", *Journal of Glaciology*, 42(140), pp. 63-76, 1996

Zirizzotti, A.; Cafarella, L.; Urbini, S., "Ice and Bedrock Characteristics Underneath Dome C (Antarctica) From Radio Echo Sounding Data Analysis," *Geoscience and Remote Sensing*, *IEEE Transactions on* , vol.50, no.1, pp.37,43, Jan. 2012

Zwally H., "Microwave emissivity and accumulation rate of polar firn", *J. Glaciol.*, vol. 18, no. 79, pp. 195–215, 1977.

5 DOMEX-3 - 2014 DATA ANALYSIS

In this section the data acquired during the campaign are analyzed. RADOMEX data analysis is presented in section 1, snow data in section 2. A short comparison to SMOS data is also contained at the end of section 1.

5.1 RADOMEX data

Data reported here were acquired continuously from December 4 2013 to December 31 2014. Some interruptions occurred during the season because of the power net failure as described in previous section.

A special attention was devoted to the calibration of the data and to some Tb fluctuations were observed in a preliminary version of the data. Three aspects were in particular treated and described in detail in the hereafter subsections.

5.1.1 DATA PROCESSING

Correction of cold load measurements

The first part of the 2014 acquisitions starts from December 2013 using the nominal operational mode which is based on the frequent calibration technique using the two internal loads at different temperatures. The obtained Tbv and Tbh uncalibrated values measured up to August 2014 trends are depicted in **Figure 23** at 42° incidence angle where the angular scan and sky calibrations have been filtered out from this analysis. The summer period (December 2013 – March 2014) is characterized by a fairly stable trend for both Tbv and Tbh with some exceptions in the period 7-13 January where an unexpected jump rises the Tb of around 5K. Daily fluctuations of the sun heating produces an oscillation in the Tbv, and the removal of this effect will be presented in details later in this section. As observed in the 2013 year the H polarization is much variable than V one because of the effect of the sun reflected from the surface toward the antenna. From the middle of March, a frequent series of Tb jumps are observed in the dataset.

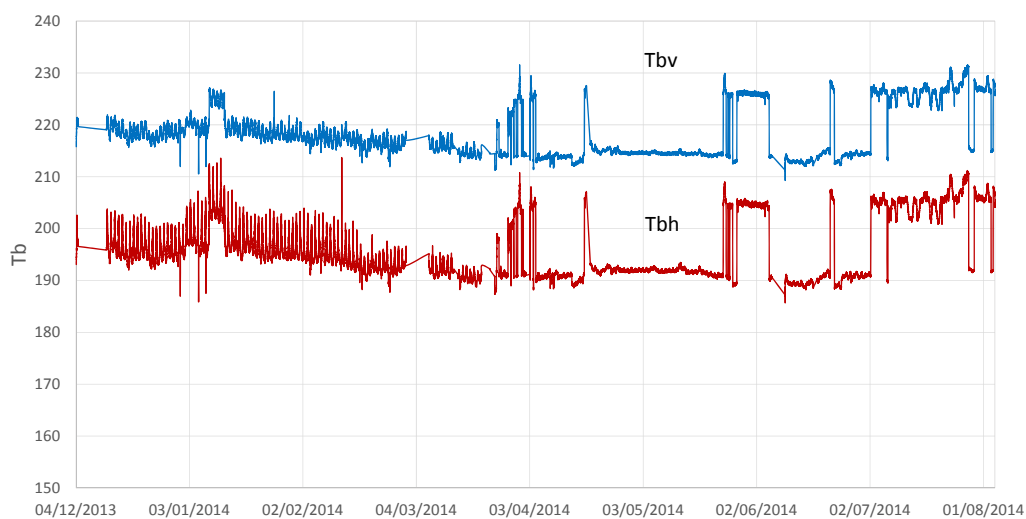


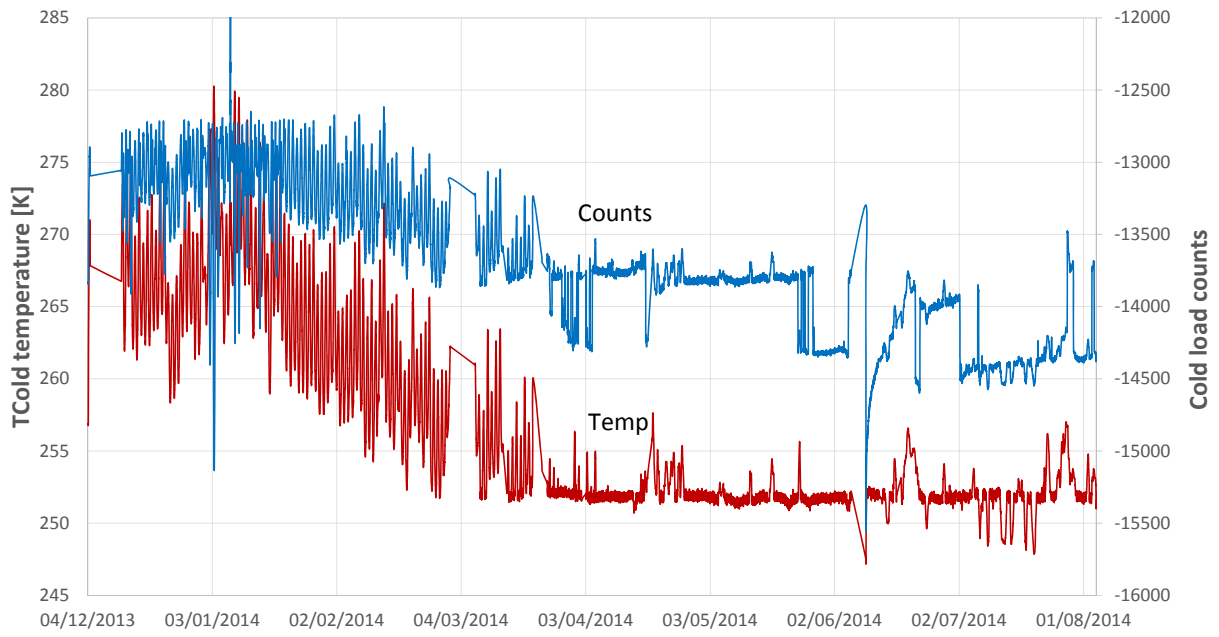
Figure 23: Temporal trend of brightness temperatures Tbv (blue) and Tbh (red) from December 2013 to August 2014 at 42° incidence.

In order to investigate which part of the radiometer is involved to the wrong estimation of the brightness temperature we focused on the RADOMEX calibration procedure which is based on the measure of the physical temperature and the brightness temperature of the reference loads. **Figure 24** shows the temporal behavior of temperature of PT100 probes and the corresponding radiometric measurements, expressed in arbitrary counts, of the cold load (**Figure 24a**) and the hot load (**Figure 24b**). The cold load counts C_{cold} clearly shows a wrong response to the temperature variations T_{cold} from the beginning of March. For instance in the period from end of May to the beginning of June the T_{cold} is pretty stable exhibiting a variation of less than 1 K while in the same period an unexpected reduction of more than 500 counts is observed. It is worth that notice that the sensitivity of the receiver is around 50 counts/1 K then. In the same period the Hot load present a regular trend as both temperature and radiometric measurements (**Figure 24b**).

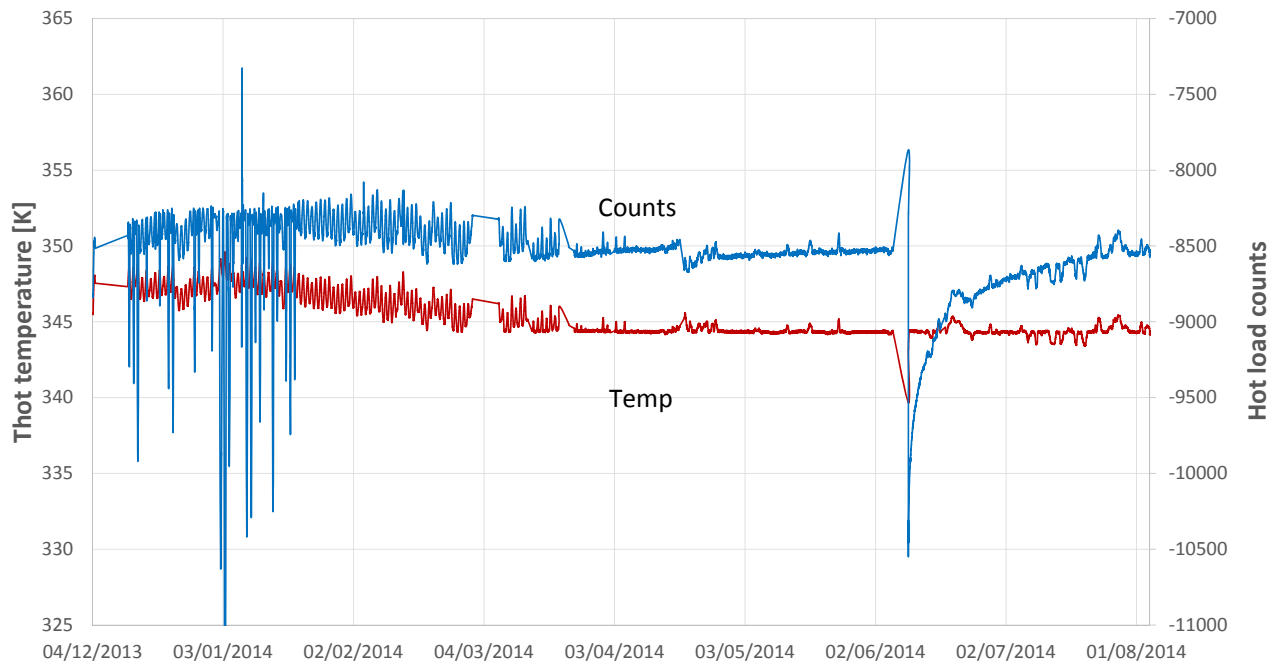
It should be remembered that the receiver is composed by a SP4T Pin switch which connects the inputs (H, V, hot and cold loads) to a RF chain (composed by filters and amplifiers followed by a detector).

Because we use the same chain for all the inputs the results observed in the hot loads confirms the good functioning of the receiver and addresses the problem to the cold load. Observing the counts of the antenna inputs (at both H and V polarization) the correct functioning of the receiver is also confirmed. In order to overcome this problem we decide to modify the operational mode and using as second reference target the noise source which is used for calibration check. The same solution was adopted during the first year of the experiment.

The T_b values corresponding to calibration failures was corrected by modifying the cold loads counts and using different methods depending on the intensity and duration of the jumps. Once a small transition of the C_{cold} counts are detected (lower than 500 counts/5days), the original counts number was removed and replaced by a value which was obtained by using a polynomial fitting that interpolate the counts value before and after the observed transition. For time intervals where C_{cold} has greater transitions (e.g. at the beginning of April and at the end of May), we assumed that the counts of the two loads are affected by the same variation because of physical temperatures changes. For this reason we attribute to the C_{cold} counts variation as a function of time the same value of the C_{hot} . An example of processed data using the above described method is shown in **Figure 25** for the period 24/6 to 3/8. Here we used both methods, the constant gain from 24/6 to 5/7 and from 26/7 to 3/8, and the fitting curve method replacing the C_{cold} transitions from 5/7 to 26/7. In the latter case, a 6th degree polynomials which better approximates the behavior of stable counts intervals was chosen.



(a)



(b)

Figure 24: Temperatures (in red) and counts (in blue) of the cold load (a) and the hot load (b) as a function of time.

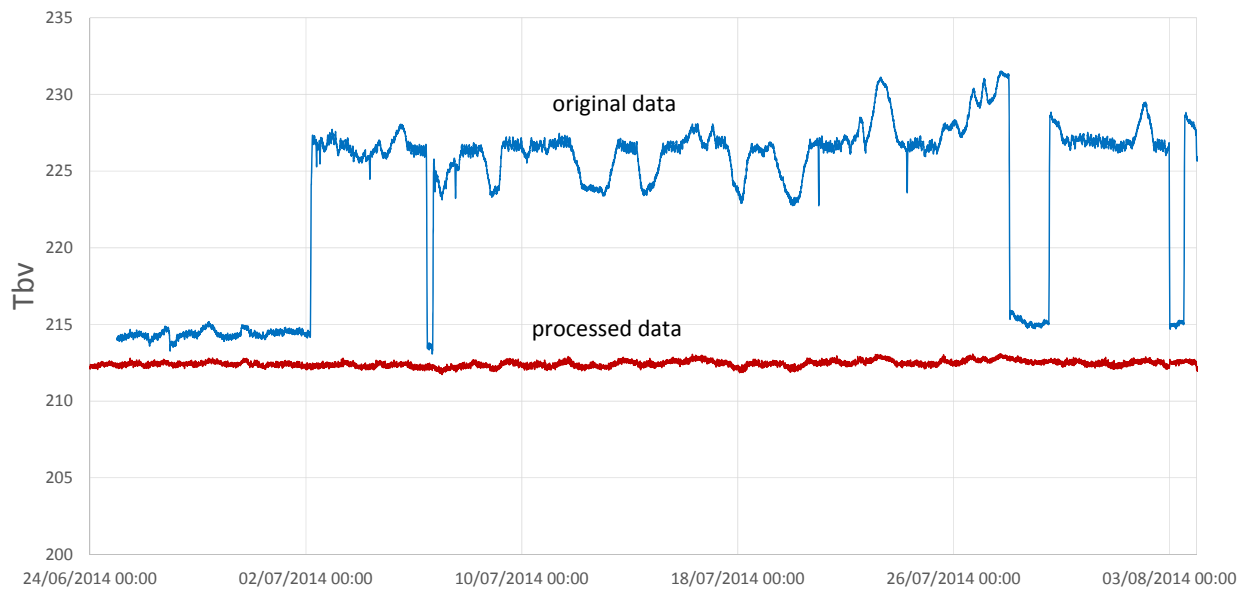


Figure 25: original Tbv corrupted from Ccold failure (blue) and reprocessed values (red) during the austral winter

Compensation of thermal effect

Once the data were corrected for this effect the whole time series (December 2013 – December 2014) was considered in order to quantify how the changes of components’ temperature affect the computation of the brightness temperature. The same procedure was already used in the first year of the campaign.

Indeed the box where the receiver and the antenna are located is thermo-controlled by an active system (based on PID and heaters) having a set-up value which is optimized for the winter period when the air temperature reaches around -90°C but cannot be maintained in summer when the temperature increases up to -25°C.

The system comprises physical devices (cables, connector, filters, switches, etc.) which are affected by thermal losses according to the Friis law:

$$T_{mis} = T_{in} L + (1-L) T_0 \quad (1)$$

Where:

Tout = temperature measured at the output of a certain section of the chain

Tin= temperature at the input of the same section of the chain

L = loss of the section

T0=physical temperature of the section

From equation (1) it can be easily understood that a variation of T0 implies a variation of the measured temperature Tout independently from the Tin. The variation obviously depends on L value.

Considering the number of devices, which compose the system, we can divide it, from a thermal point of view, in two main areas: a “cold” area outside to the receiver box composed by the antenna cables and connectors, and a “hot” area internal to the receiver.

This leads to a relationship from the antenna temperature T_a to the receiver inputs T_b as:

$$T_b = (L_1 T_a + (1-L_1)T_1) L_2 + (1-L_2) T_2 \quad (2)$$

Where L_1, L_2 and T_1, T_2 are the losses and the temperatures of the first and second part.

In order to correct this effect we compute the L_1 and L_2 values which minimize the temporal standard deviation of the T_a computed over a certain period of few days computed as:

$$T_a = \frac{T_{bv} - (1-L_2)T_1L_1 - (1-L_1)T_2}{L_1L_2} \quad (3)$$

The assumption of this approach is that the ice sheet emissivity does not change as average value in a short time period.

For the V polarization we consider all the data while for H polarization we considered only the points where the effect if sun reflected doesn't affect the data (i.e. the sun is in the opposite direction respect to the tower).

Because of the dependence of eq. 2 by both T_b and $T_{1,2}$ we first investigated on the temporal shift between the two quantities in different period of the year, which could compromise the quality of the correction. Indeed temporal shift can differs in the different period of the year since in winter the temperature of the whole system is well stabilized while is more unstable in summer. In order to better explain the this effect, we first represents the temperature measured in the receiver chain near to the noise source called T_{ns} (**Figure 26**). We identified three different periods, one in summer **Figure 27** (a) corresponding to the highest T_{ns} fluctuations, and the others with a stable T_{ns} **Figure 27** (b)-(c) in February and March. We found that the time shift of T_b/T_1 is of around 2h in the first period and 1 hours in the second period. The same value was obtained in the third period where the system temperature was not changed.

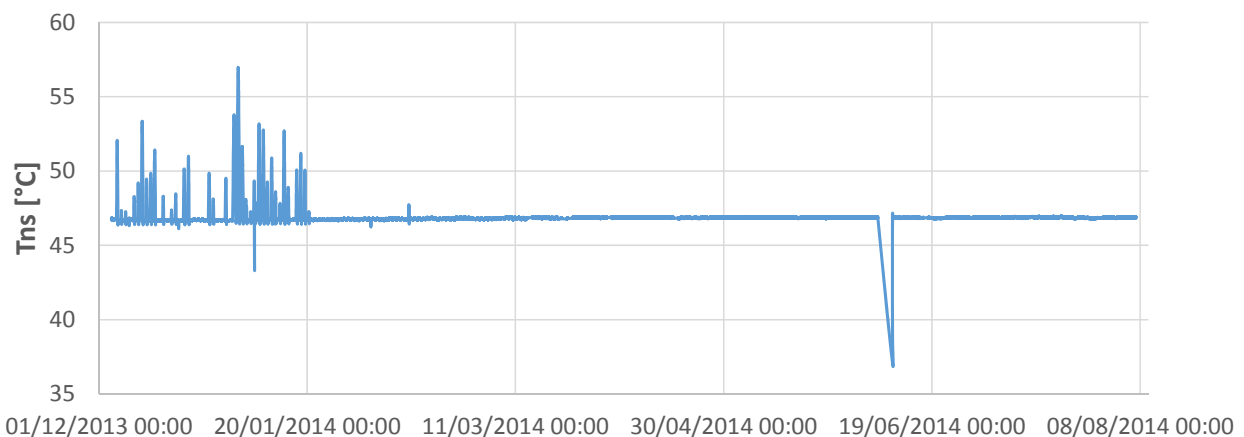
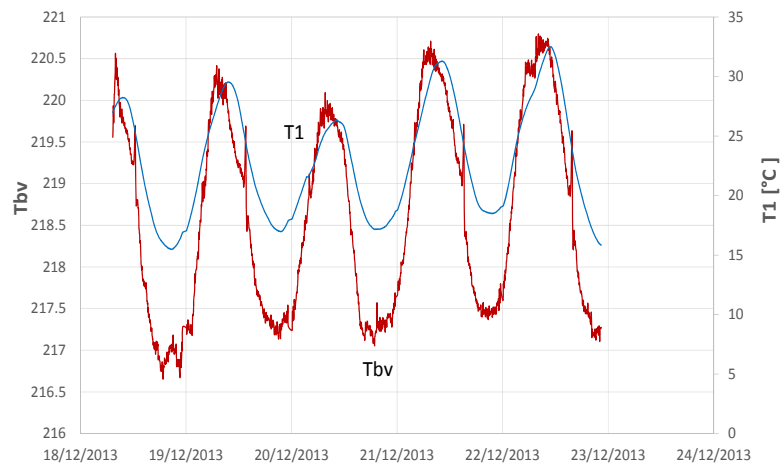
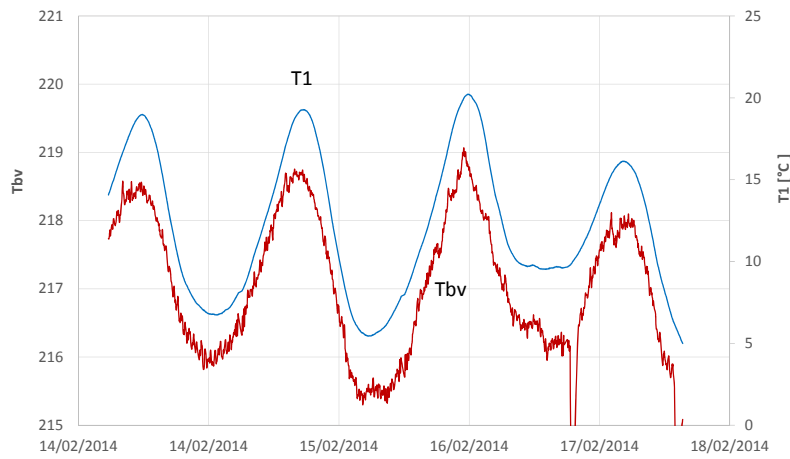


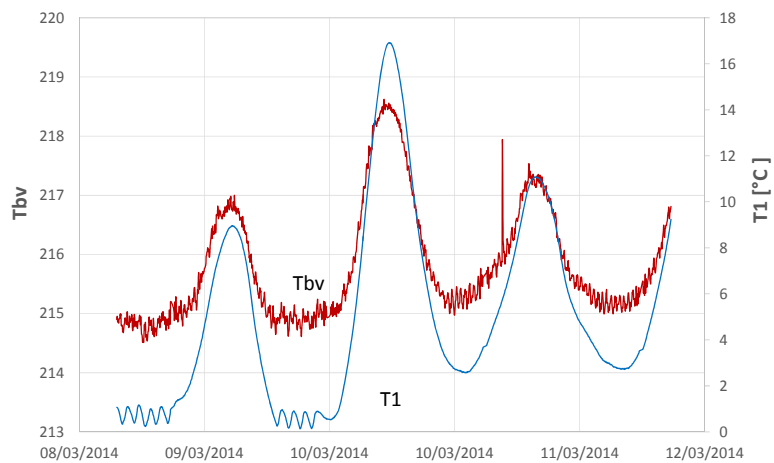
Figure 26: Temperature internal to the system T_{ns} .



(a)



(b)



(c)

Figure 27: Time shift between Tbv (red) and T1 (blue) for three different periods of the year, (a) for fluctuating Tns, (b) - (c) for stable Tns.

Absolute T_{bv}/T_1 shifts as well as the relative ones for each period were delayed in order to obtain zero shift, and used as input for eq. (3).

As an example we compare in **Figure 28**, a corrected T_b value (not absolutely calibrated) using the original data of **Figure 27 (a)** and the second after T_{bv} re-phasing (shift=0). The improvement of the shift removal is pretty clear, and the RMSE decreases from 0.6 K to 0.36K. Remaining fluctuations are due to secondary effects which were not yet considered.

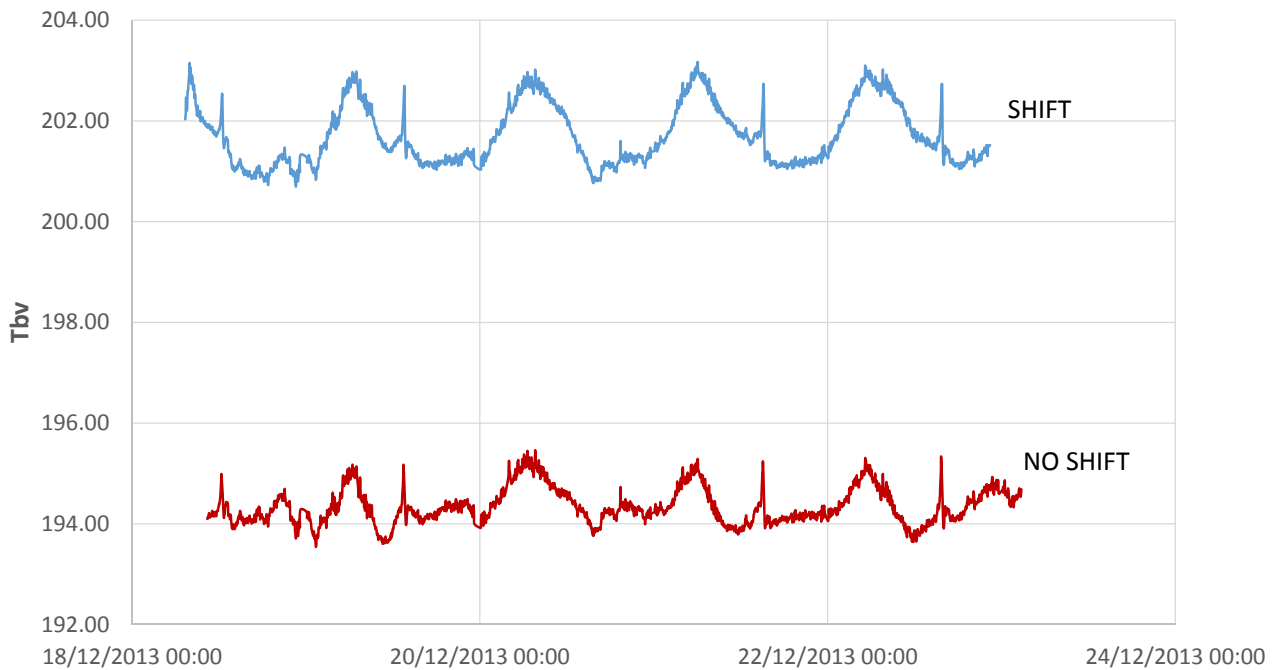


Figure 28: Time shift effect on the T_{bv} correction showing the original case with T_1 shift (blue) and the re-phased one (in red).

The method was then applied to the whole 2014 dataset, finding for each period the optimum values of L_1 , L_2 . As an example **Figure 29** shows a 12 days period during austral summer where T_b is calculated before and after the correction, for both V and H polarization. Optimum values for the couple (L_1 , L_2) (antenna/switch and switch/receiver respectively) are (0.81, 0.99) for the V pol. and (0.85,1) for the H pol. For the V case, the daily fluctuation is reduced and the peak-to-peak dynamic passes from 5.3K to 1.5K while the mean square error RMSE drops from 1.53K to 0.54K. For the H- pol, the correction does not reduce daily temperature effect (sun effect is observed for the H-pol) but removes the longer scale variation of T_1 and T_2 , yielding minimum values nearly constant for the whole period. This effect is also weakened for V polarization (**Figure 30**).

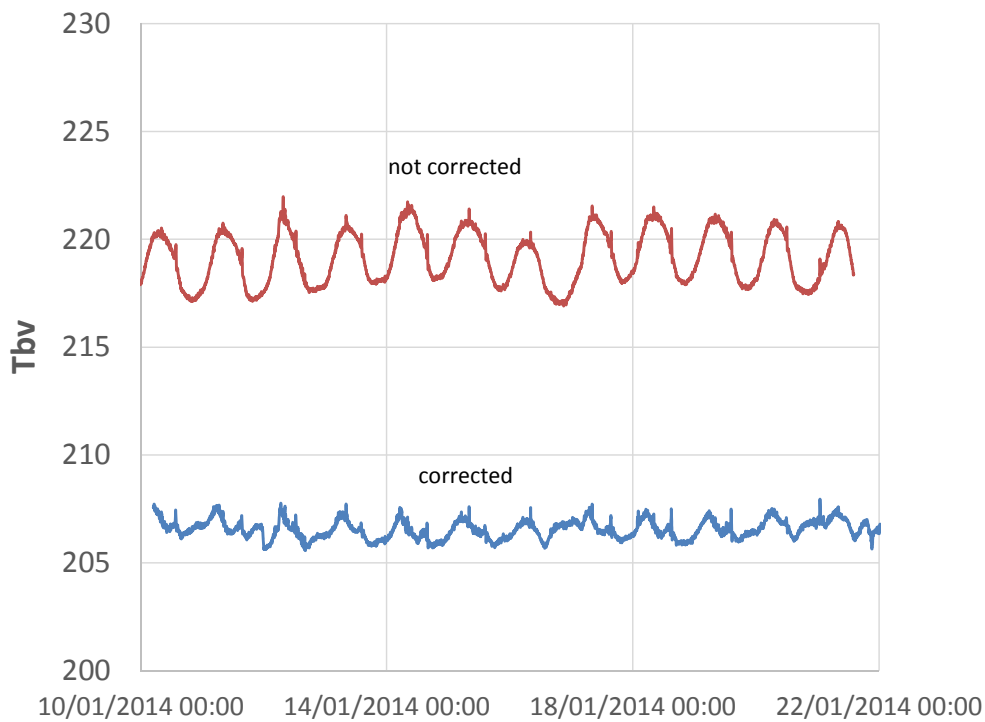


Figure 29: Temporal behavior of the Tbv before the temperature correction (red) and after the correction (blue).

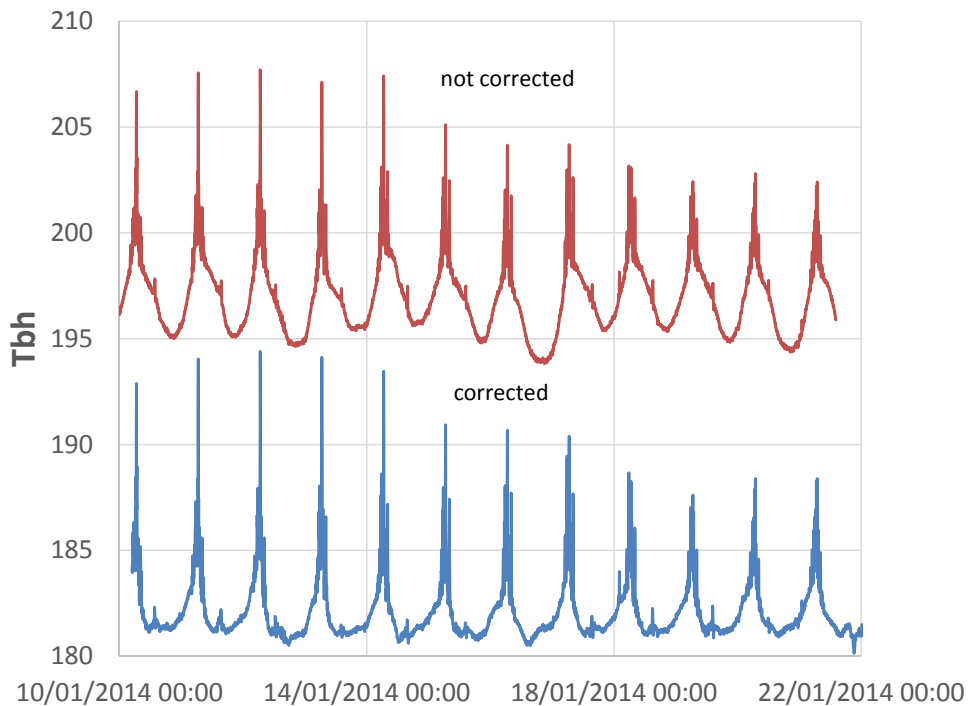
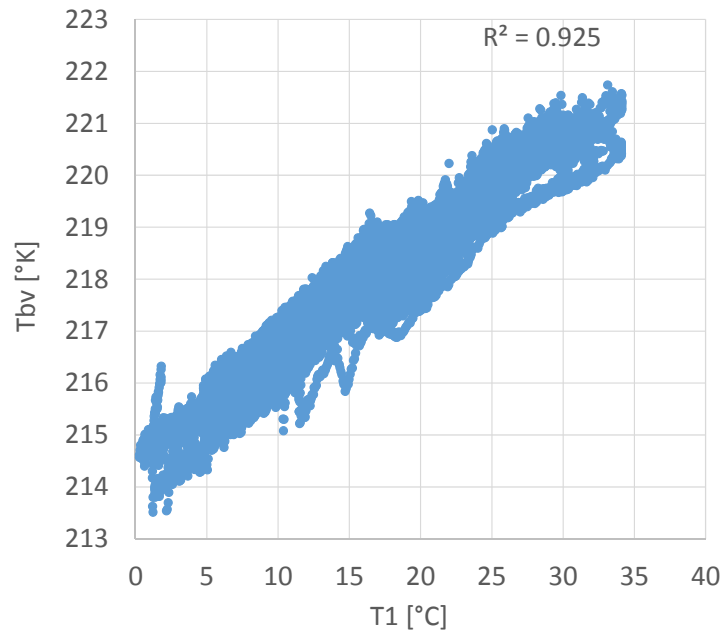


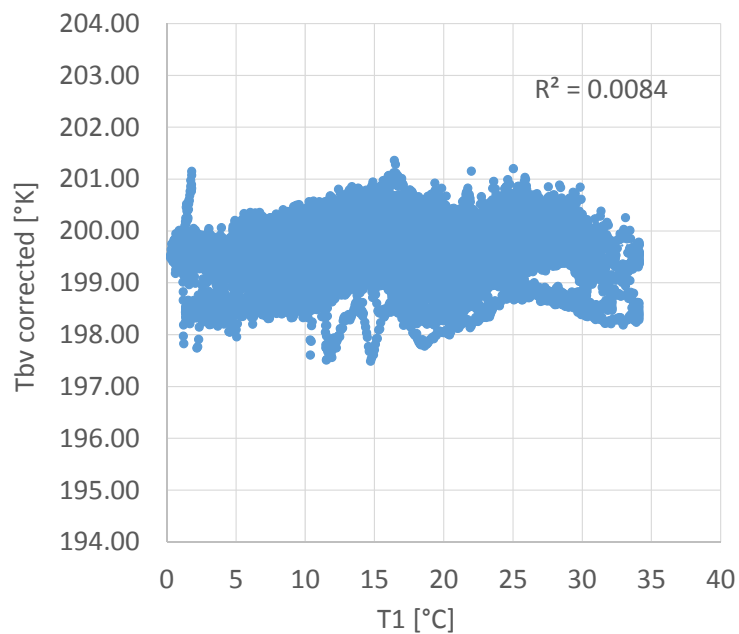
Figure 30: Temporal behavior of the Tbh before the correction (red) and after the correction (blue).

In order to quantify the introduction of the correction of the cable temperature effect, the determination coefficient between Tbv and $T_{1,2}$ was computed and reported in Figure 31 for the period December 2013-February 2014 before and after the procedure. The correlation of the two quantities drops from 0.92 to

nearly 0 after the correction demonstrating that the adopted procedure strongly reduce the dependency to the devices' temperature.



(a)



(b)

Figure 31: Correlation between Tbv and cable temperature T1, before the correction (a) and after the correction (b).

The minimization provides different combinations of L_1 and L_2 , estimated for different periods of the year. Collected values were analyzed as a function of the mean temperature of the cables for each period and reported in Figure 32. At V polarization L_1 shows a decreasing function of the temperature, ranging from 0.95 to 0.81 while L_2 is nearly stable with a minimum value of 0.99. Similar results were produced for the H pol. It is worth pointing out that, because of the high thermal excursion of the cables, the estimates of L does not provide real values of the cable loss but a general value to minimize the thermal fluctuation effect. Higher order effects (e.g. switch and junction losses, mismatches) will be included in future analysis. However, this preliminary correction is effective for the purpose of this study.

At the end of the analysis a coherent and homogenous data sets was obtained and is described in detail in the following section.

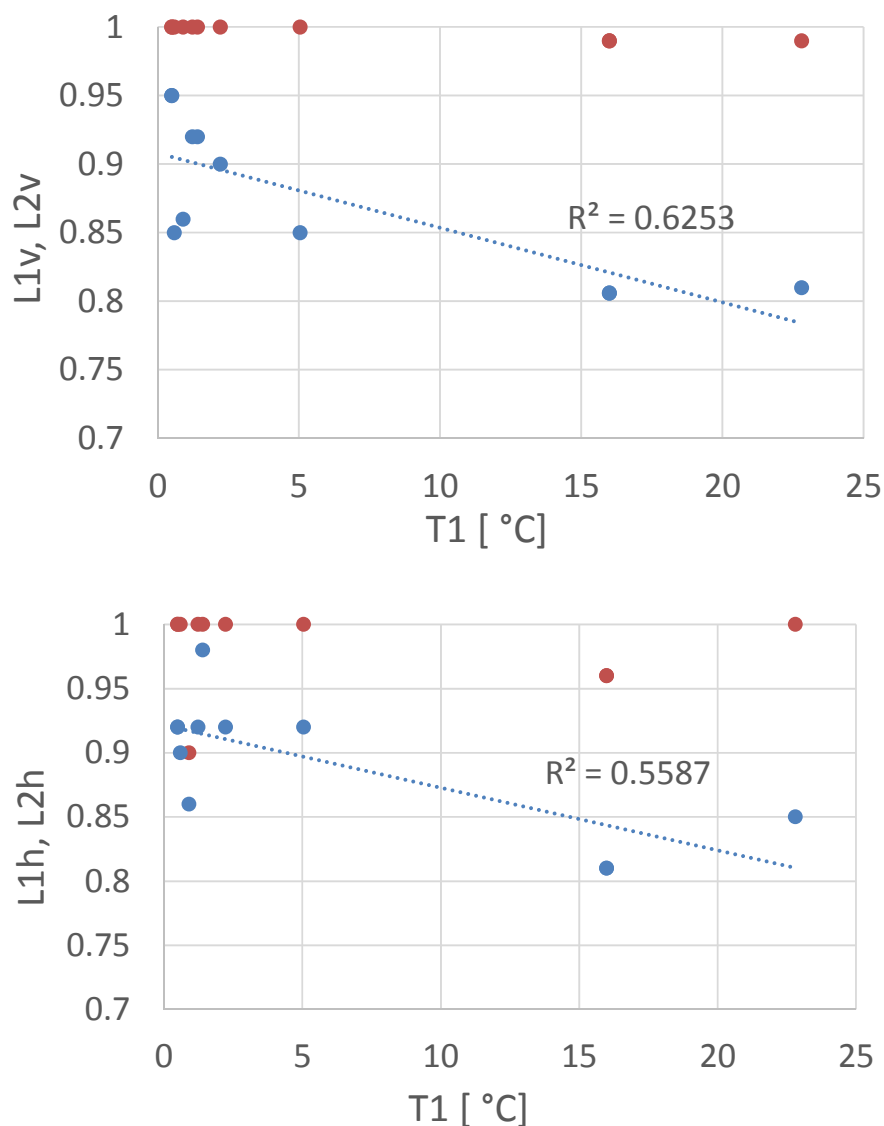


Figure 32: L as a function of T_1 estimated for (top) V-polarization and (bottom) H-polarization. Blue and red markers represents L_1 and L_2 respectively.

5.1.2 DATA ANALYSIS

The brightness temperature was acquired in the whole considered period after the processing is represented in Figure 33 at V (blue) and H (red) polarization. Low temperature Tb values (i.e. near to zero) observed in some period of the year represent data acquired observed on the sky for calibration check while high Tb values (i.e. higher than 300K) measured at the beginning of the period represent measurements were performed over matched load (i.e. without antenna) again for calibration check. In general, as in the previous years, we can observe that V polarization is more stable than H polarization. In addition H polarization presents several peaks during the summer season which are caused by the sun reflected on the surface and observed by the radiometer as pointed out in the first year report [6].

It is also worth noting that the strong RFI peaks observed during the first year at V polarization are not here detected.

In processing the H polarization data were collected at 42° of incidence angle it was decided to eliminate them if the azimuth position is higher than 200° or lower than 100° when the sun is higher than the horizon.

Data collected at 42° of incidence angle after the removing of data were affected by the sun are shown in Figure 34.

It can be observed that data at V polarization are very stable while H polarization presents some fluctuations. In particular a significant drop of around 3 K is observed at end of February when Tb moves from to 187 K to 184 K and then tends to increase in the following period.

The mean values at V and H polarizations are 207.56 K and 185.89 K respectively and the correspondents standard deviation 0.39 K and 0.69 K. These data are in a quite agreement with data acquired during the first year when the mean values were 207.41 K at V and 185.36 at H polarization respectively.

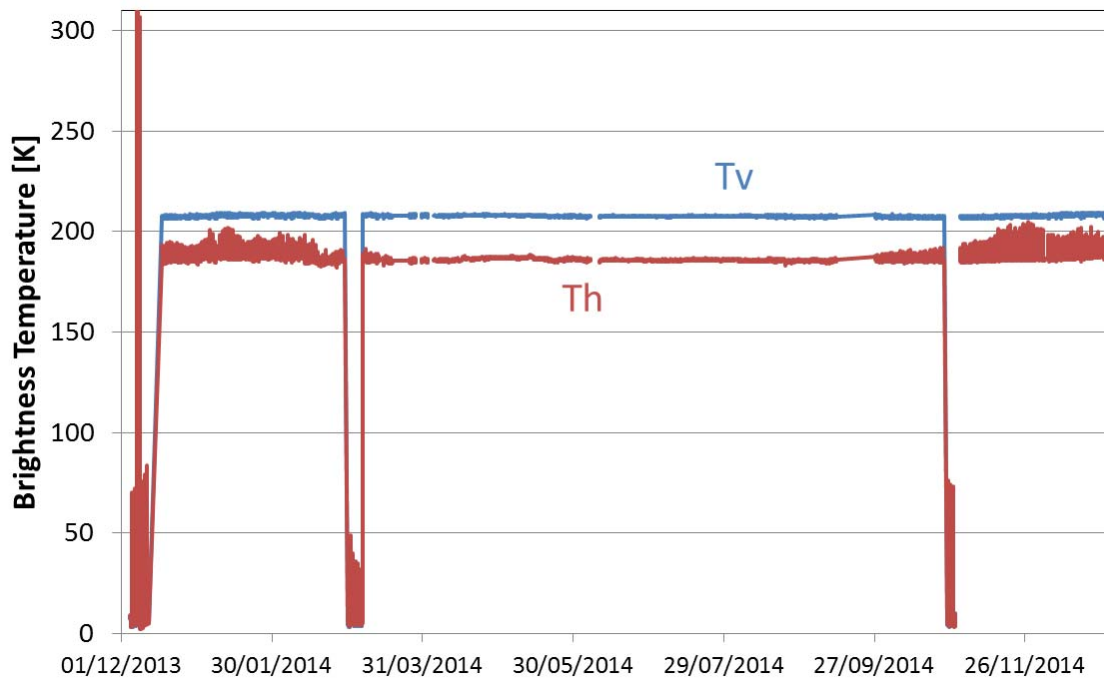


Figure 33 Brightness Temperature at V (blue) and H (red) polarization as a function of time for the whole considered period

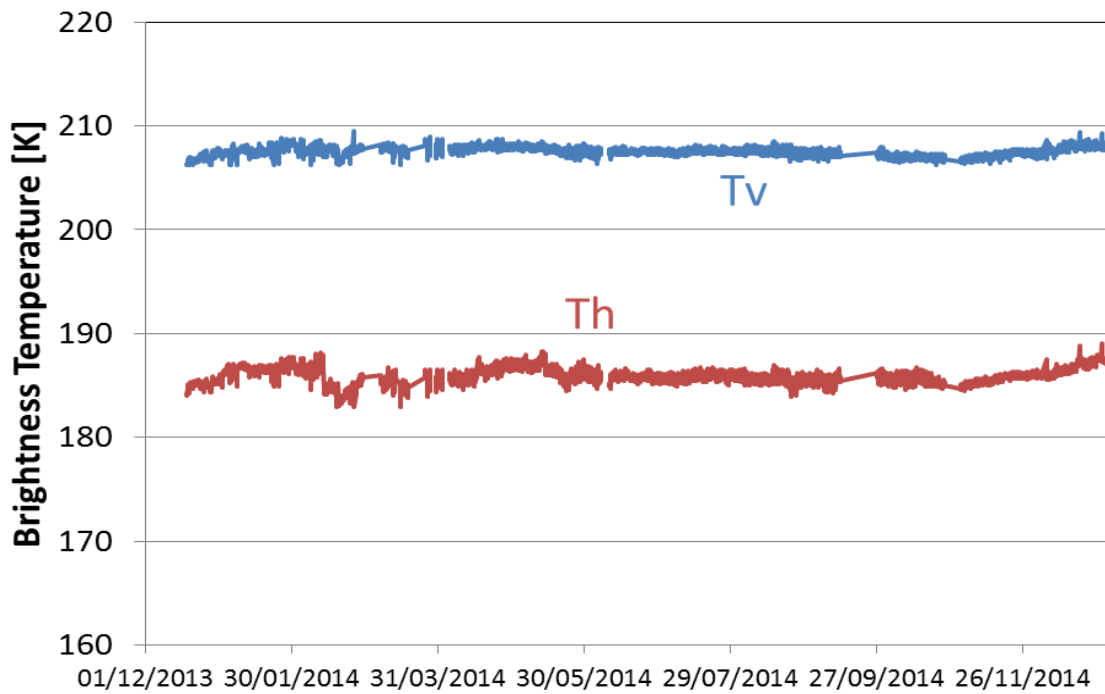


Figure 34 Brightness Temperature at V (blue) and H (red) polarization as a function of time for the whole considered period at 42° of incidence angle and after removing the sun effect.

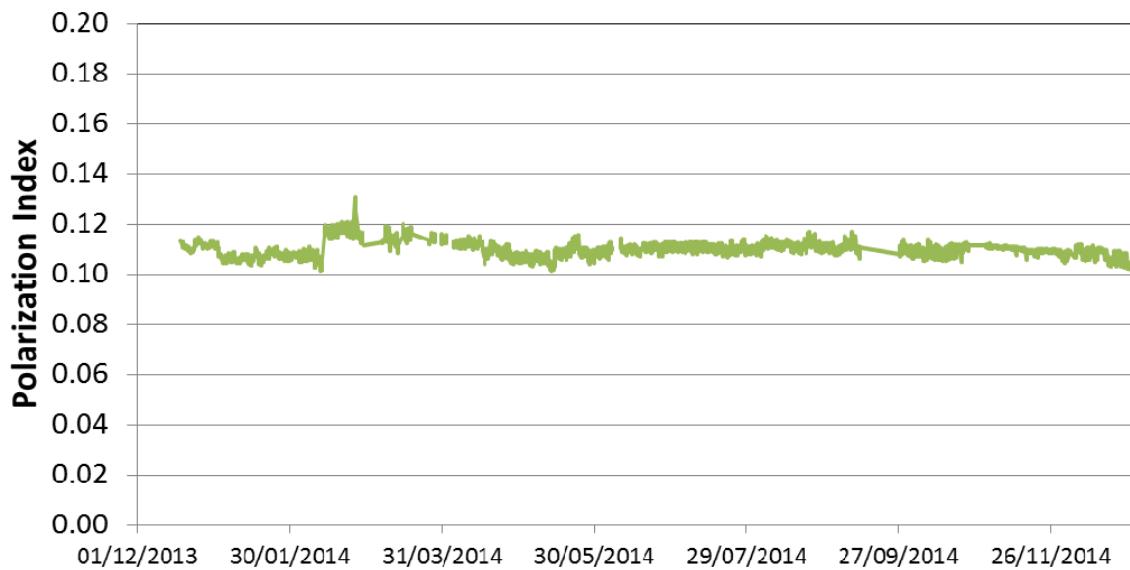


Figure 35 Polarization Index as a function of time.

For the same period the polarization index PI ($PI = 2 * (T_{bv} - T_{bh}) / (T_{bv} + T_{bh})$) is represented in Figure 35. PI remains quite stable in time showing only a variation (i.e. initial decreases and a subsequent increases) at the beginning of the experiment because of the modification of TbH. The PI mean value is 0.110 and its standard deviation is 0.0028. Also these values are fully in line to data observed in first year of 0.112 and 0.0028.

Some tests were performed in order to evaluate the quality of the data. In particular the calibration stability of the radiometer was checked along the season using the measurements were occasionally collected on hot and cold reference targets. This verification is particularly important since, as above mentioned, the calibration scheme was modified during the experiment. Moreover, as previously explained the data were processed by using a modification of attenuation parameters and the time delay between temperatures along the years.

As an example data collected on different periods on clear sky, which is used as cold reference, are shown in **Figure 36**. The peaks on the Tb data corresponds to the period where the sun were directly observed by the antenna. It can be observed that data are quite consistent in the 3 time periods of the year. Moreover, in the diagrams it can be nicely observed second minor peaks, before or after the sun ones, caused by the observation of the plan of the galaxy by the antenna. Comparison between these values and theoretical ones will be further investigated. The Tb values, and the corresponding standard deviation, for the three periods were represented in Table 5-1. In table the Tb value represents the average value computed when the sun doesn't affect the measurements. Tb measured on the sky is quite constant along the years, the difference between the periods along the years is on the order of 0.5 K, confirming the goodness of the processing and calibration scheme. Also the difference between the two polarizations is less 0.3 K. Data are also full in agreement to what observed during the first year of the experiment.

At the beginning of the year, a test was conducted connecting a matched load to the antenna cable and measuring its temperature for some days in order to verify the calibration over high brightness temperature values. An example of one of these time series is presented in Figure 37.

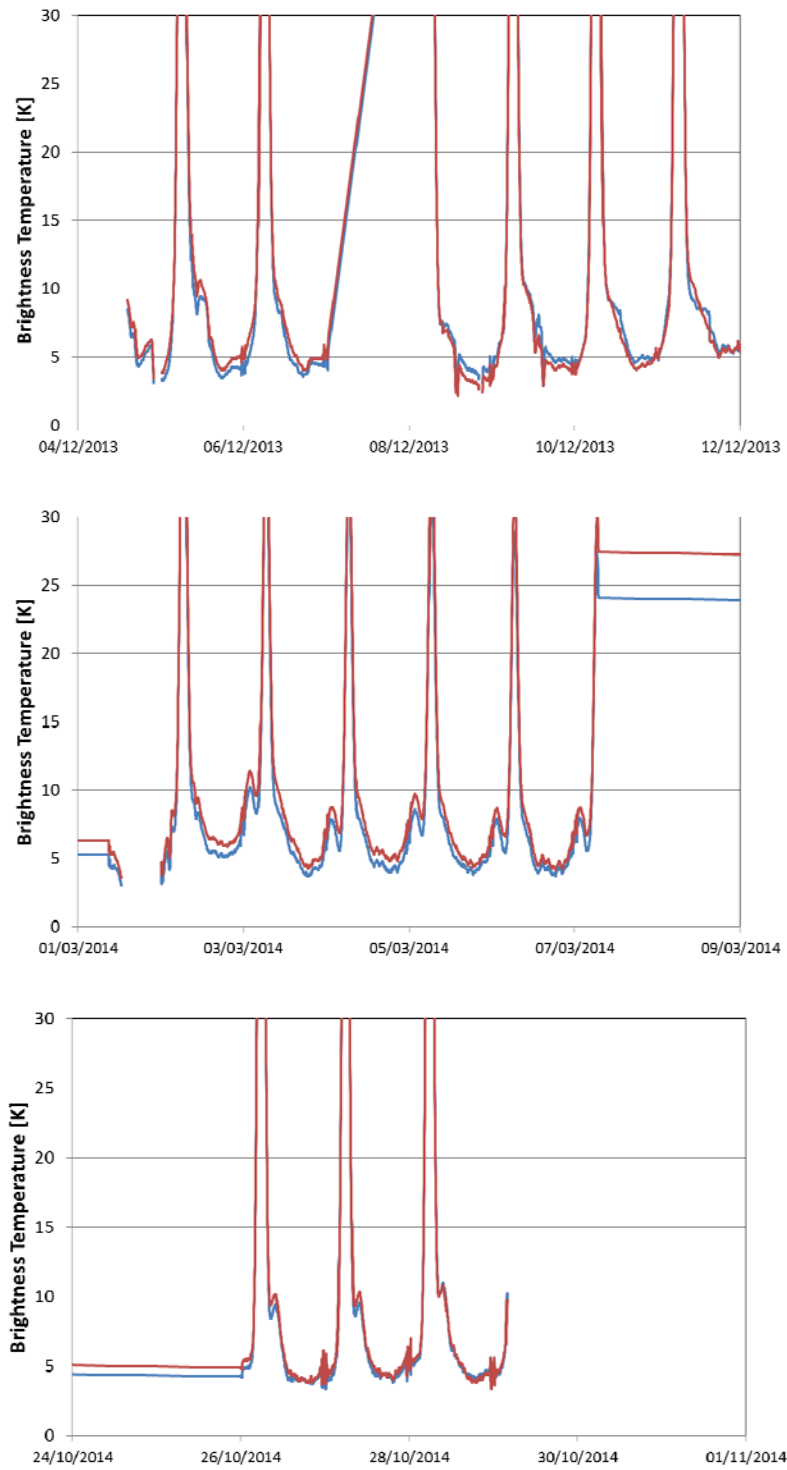


Figure 36 Brightness Temperature measured on sky at V (blue) and H (red) polarization.

In order to verify the calibration level over a broad brightness temperature range, data collected during the year (March 2014) at different incidence angle in the range 30-70 degrees are compared to data acquired in 2013 and during DOMEX-2 (Figure 38). Figure demonstrates that Tb remain quite stable in time exhibiting the same values in the 130 -210 K range.

Table 5-1 – Measurements Collected on Clear Sky

	TbV (K)	Std (K)	TbH (K)	Std (K)
December 2013	4.62	0.70	4.53	0.79
March 2014	4.5	0.66	4.70	0.76
October 2014	4.15	0.20	4.13	0.20

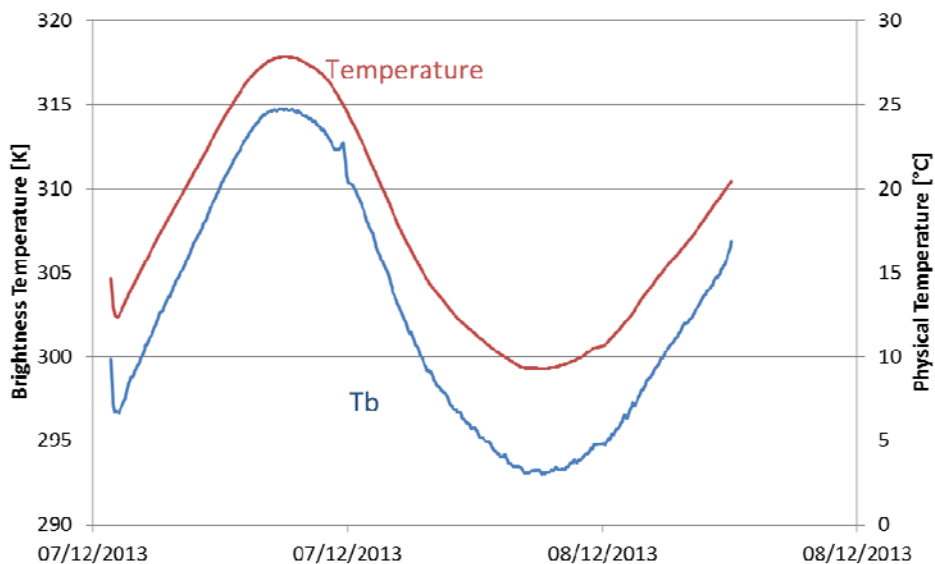


Figure 37 Brightness Temperature at V polarization (blue) and matched load temperature (red) as a function of time.

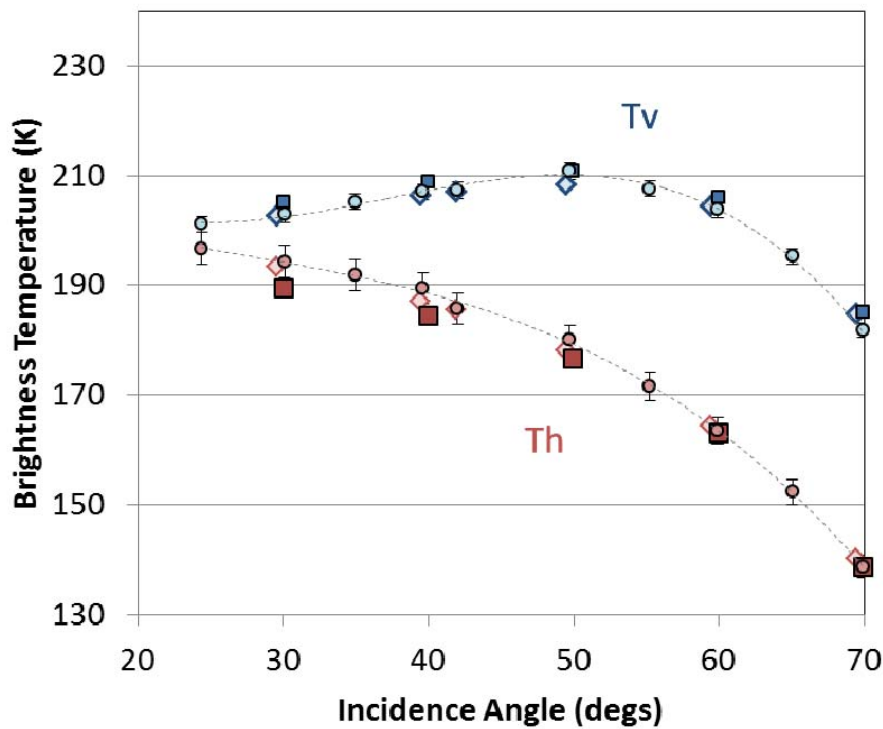


Figure 38 Brightness Temperature at V and H polarization as a function of incidence angle. Blue = V polarization: circle 2013 data, Diamond – 2014 data, square DOMEX 2 data. Red = H polarization : circle 2013 data, Diamond – 2014 data, square DOMEX 2 data.

Additional checks were performed in order to evaluate the data quality and the receiver's performances. First of all the standard deviation of T_b , obtained every 3 minutes of acquisition, is represented in **Figure 39**. The standard deviation value is quite stable over time and is around 0.3 K as mean value although some peaks are observed for specific periods.

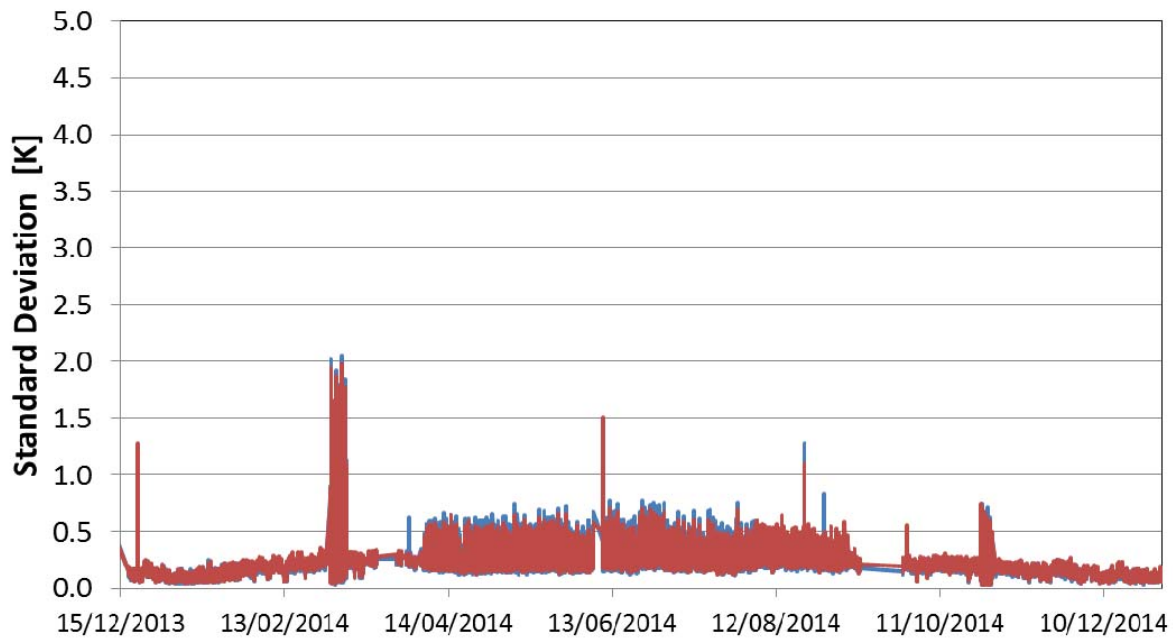


Figure 39 Brightness Temperature standard deviation at V (blue) and H (red) polarization as a function of time

Temperature of the receiver was also measured during the experiment in several points. Figure 40 points out that the temperature of the receiver’s chain remains very stable in time exhibiting a temperature stability better than 0.1 °C over several months. The antenna’s cable temperature is more unstable since it is affected by air temperature variation which exhibit a daily fluctuation of around 12°C and an annual variation of more than 60 °C.

Figure 41 shows the temperature of the antenna’s cable and RF’s cable as a function of time. The temperature fluctuates of around 5/6 °C with respect to its mean value. This latter varied during the experiment because of the decreases of air temperature. As expected during the winter period the data are more stable.

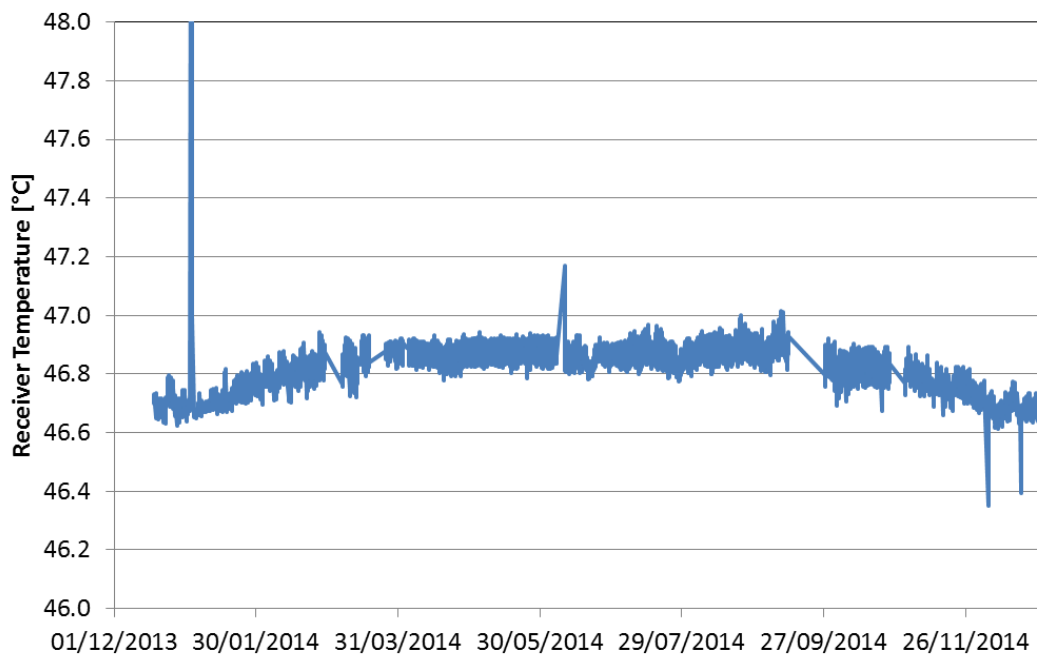


Figure 40 Temperature of the RF receiver as a function of time.

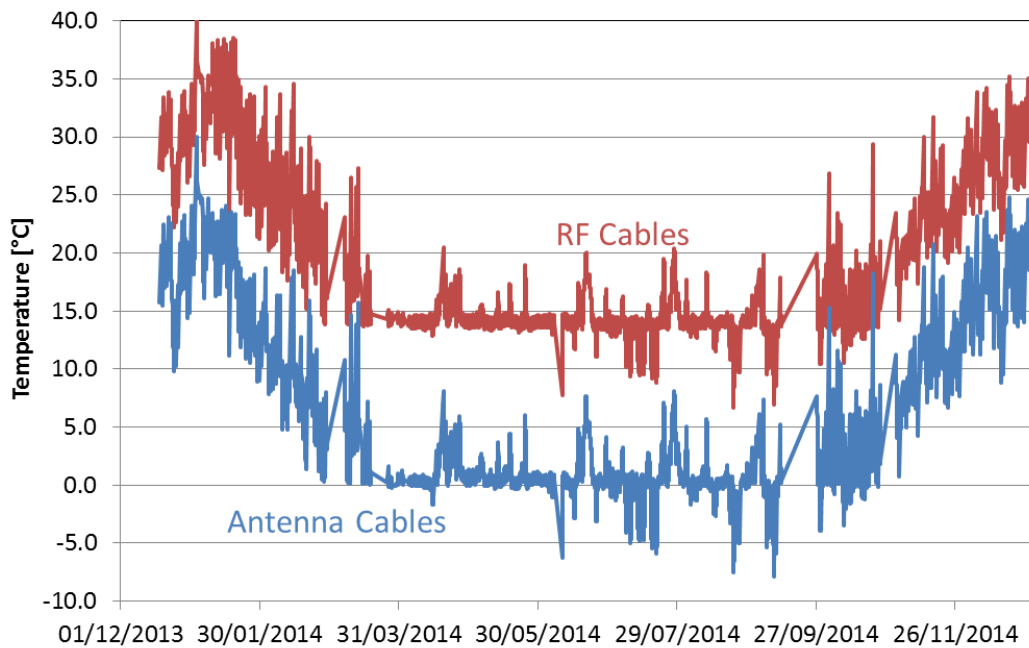


Figure 41 Temperature of the antenna's cable as a function of time.

5.2 Comparison to SMOS data

A preliminary comparison between SMOS and DOMEX-3 data is presented here.

SMOS, Level 1C data version 620, provided by ESA were used in the analysis. The following criteria were used in the selection of data:

- Data collected from December 2013 to December 2014 were considered
- observations from the 'alias-free' FOV of the overall SMOS footprint were used.
- data with sun, moon, galactic glint, or RFI flags set were discarded.
- only data with Earth incidence angles of 42 ± 2.5 degrees were used for temporal analysis
- polarization was rotated from x-y coordinates to H-V using SMOS tools.

The comparison between the two data sets ,Figure 42 , shows that the two data sets are in a very good agreement as temporal trends despite the different size of the areas observed by the two sensors was very different (i.e. hundreds meters by Radomex and tens kilometers by SMOS). SMOS vertical polarization are higher than RADOMEX of around 4 K moreover RADOMEX data reported here are not deconvoluted and a bias of +2.2 K was observed in the new version of SMOS data (V620) with respect to the previous one (V505). As observed in previous comparison SMOS data are much noisier than Radomex exhibiting a standard deviation of around 3K.

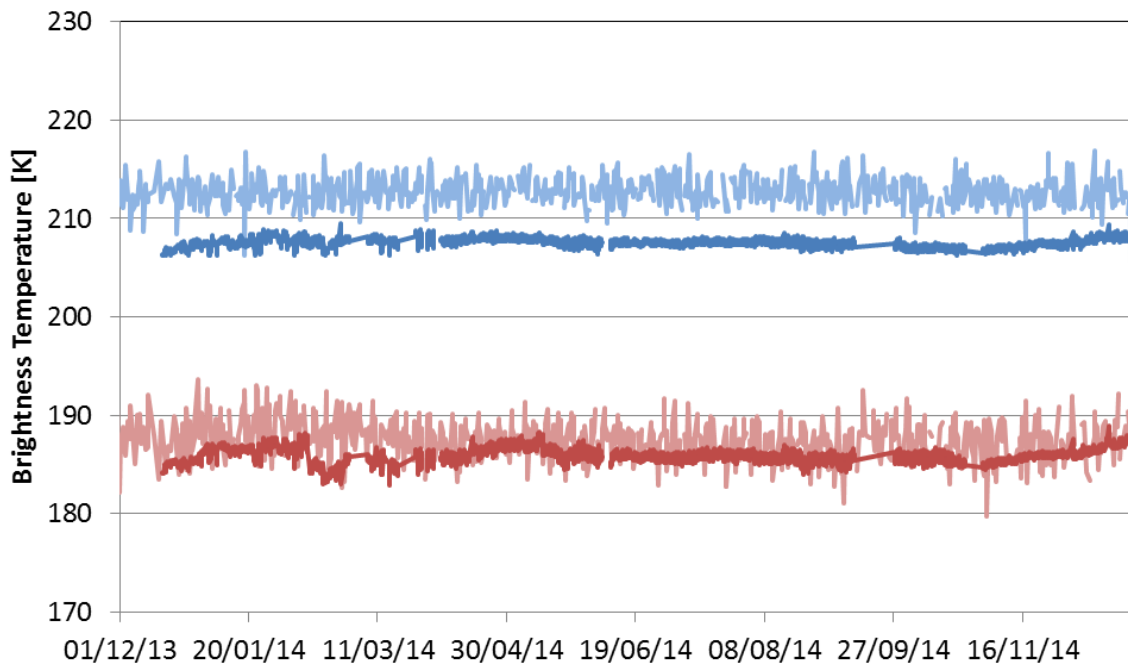


Figure 42 - Measured Brightness Temperature, incidence angle 42° , as a function of time at V (blue) and H (red) polarization by SMOS (light color) and RADOMEX (dark color) for year 2014.

5.3 SNOW Data

Snow measurements were carried out during both the summer and winter campaign. Obtained results are briefly summarized here.

5.3.1 Snow temperature

The snow temperature at different layer was monitored also during the year, by means of permanent snow probes located in Concordia Base. The depth of the probes is the following: 5, 10, 25, 75, 100, 150, 200, 250, 300, 400, 500, 600, 800 and 1000 cm.

Figure 43 presents the snow temperature in the period 2014 acquired at different depths. As obvious the trend of the snow temperature at 100 cm is influenced by the variability of the air during the year, while at higher depths the temperature is very stable.

Mean and standard deviation snow temperature at the different depths are show in Figure 44. As expected the mean values are constant in time while the standard deviation decreases as the depth increases.

The IR temperature is also represented in **Figure 45**

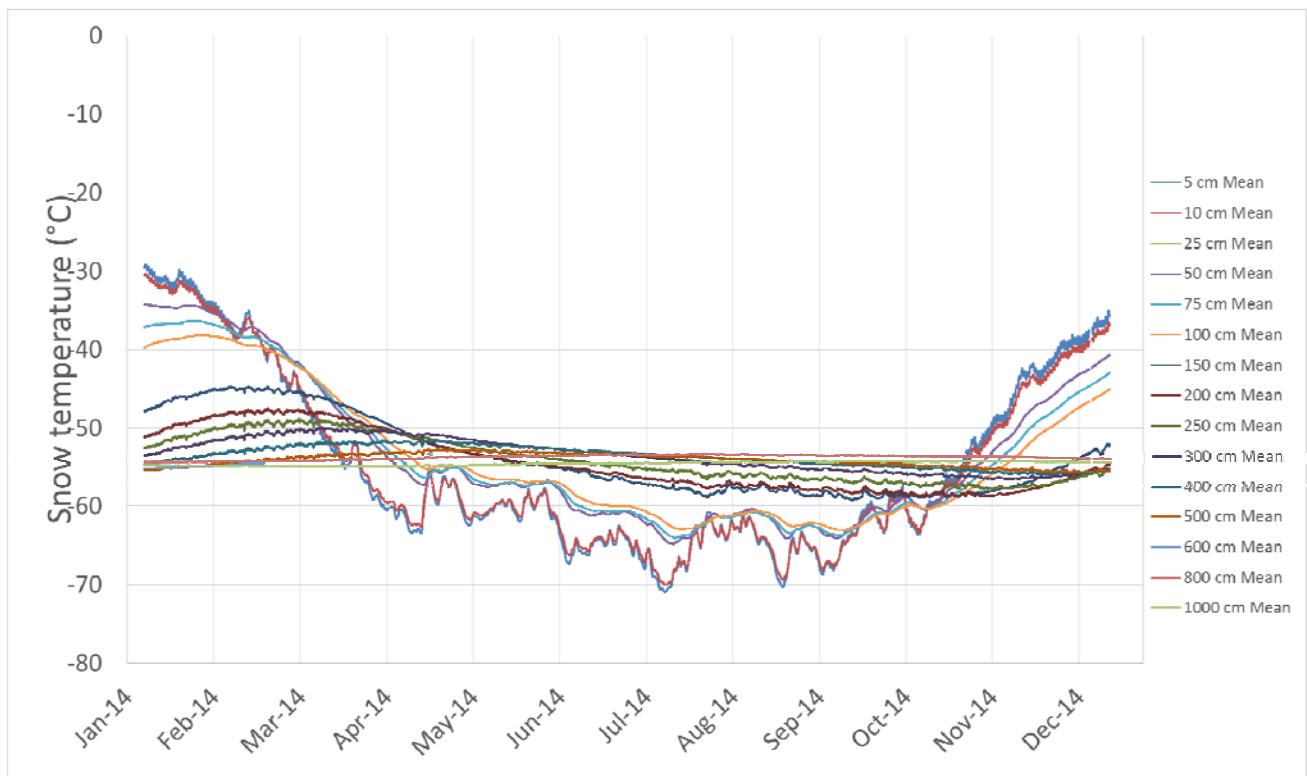


Figure 43 - snow temperature at different depths measured in 2014 year

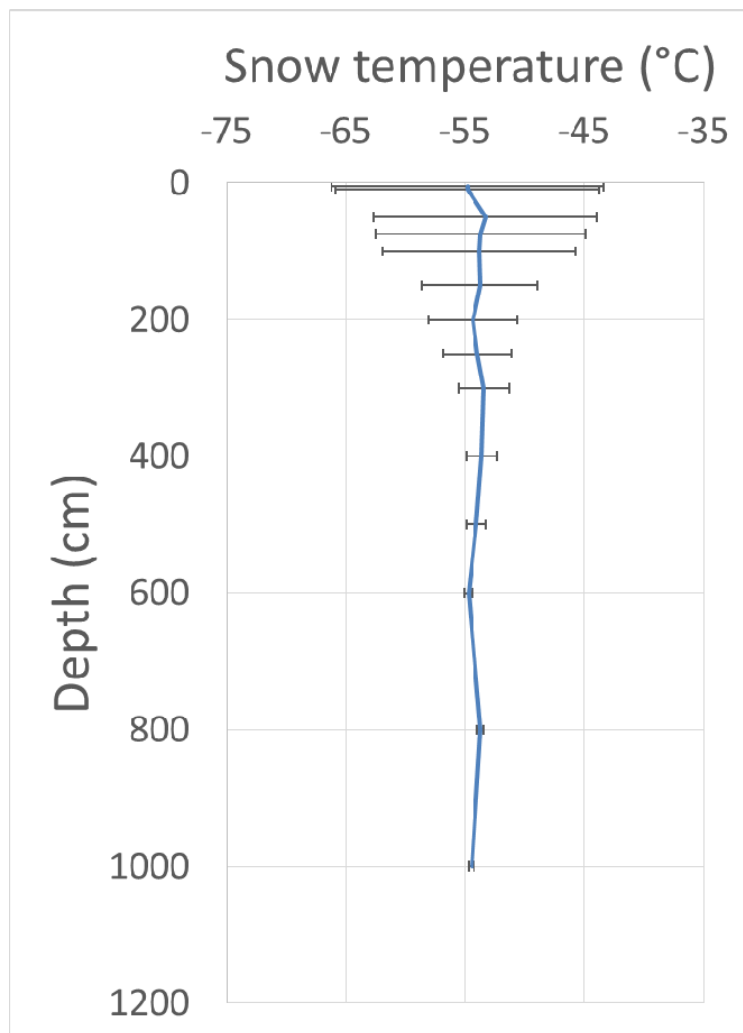


Figure 44 - Average and standard deviation of the snow temperature as a function of depth for year 2014.

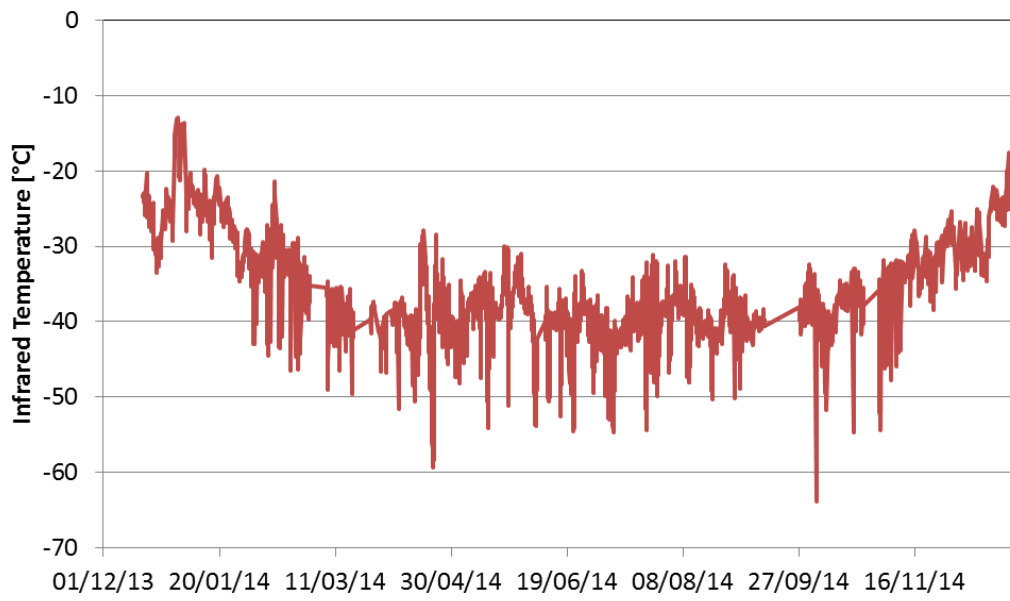


Figure 45 - Infrared temperature.

6 References

- [1] ESA-contract Technical Support for the Deployment of an L-band Radiometer at Concordia Station, Final Report, 2005
- [2] ESA Contract:20066/06/NL/EL 22046/08/NL/EL, - Technical Support for the Deployment of an L-band radiometer at Concordia Station during DOMEX-2- - Final Report . 2011
- [3] Esa Contract: 4000105872/12/NL/NF - Technical Support for the Deployment of an L-band radiometer at Concordia Station during DOMEX-2 – Proposal –July 2012
- [4] Esa Contract: 4000105872/12/NL/NF - Technical Support for the Deployment of an L-band radiometer at Concordia Station during DOMEX-2 – Campaign Implementation Plan, Deliverable D2 – October 2012
- [5] Esa Contract: 4000105872/12/NL/NF - Technical Support for the Deployment of an L-band radiometer at Concordia Station during DOMEX-2 – Readiness Review Report, Deliverable D3 – October 2012
- [6] ESA-ESTEC Contract 4000105872/12/NL/NF Technical Support for the Long-Term Deployment of an L-Band Radiometer at Concordia Station, First Year Report , D6, February 2014
- [7] ESA Contract 18060/04/NL/CB - Technical Support for the Deployment of an L-band radiometer at Concordia Station Final Report . May 2006

TECHNICAL SUPPORT FOR THE LONG-TERM DEPLOYMENT OF AN L-BAND RADIOMETER AT CONCORDIA STATION

DATA DESCRIPTION: MW –IR TEMPERATURE

JUNE 2015

EUROPEAN SPACE AGENCY STUDY CONTRACT REPORTS

ESTEC CONTRACT 4000105872/12/NL/NF

PREPARED BY

Giovanni Macelloni, Francesco Montomoli and Marco Brogioni

IFAC – CNR – SESTO FIORENTINO – ITALY

DATE:

June 2015



This page is intentionally left blank

ESA STUDY CONTRACT REPORT			
EUROPEAN SPACE AGENCY STUDY CONTRACT REPORTS ESTEC CONTRACT 4000105872/12/NL/NF	TECHNICAL SUPPORT FOR THE LONG- TERM DEPLOYMENT OF AN L-BAND RADIOMETER AT CONCORDIA STATION		CONTRACTOR: IFAC-CNR
ESA CR ()No:	STAR CODE:	No of volumes: 1 This is volume no: 1	CONTRACTOR'S REF: MW-IR Temperature DataBase
<p>ABSTRACT:</p> <p>This report contains the information of the MW-IR temperature data collected during DOMEX-3 experiment.</p>			
<p>The work described in this report was done under ESA Contract. Responsibility for the contents resides in the author or organisation that prepared it.</p>			
<p>AUTHORS: G. Macelloni, M. Brogioni, F.Montomoli (IFAC-CNR) ,</p>			
ESA STUDY MANAGER: T.Casal		ESA BUDGET HEADING	

This page is intentionally left blank

1 TITLE

1.1 Data set identification

DOMEX-3 Microwave and Infrared Radiometers data

1.2 Revision date of this document (yy/mm/dd)

11/06/2015

1.3 INVESTIGATOR(S)

Dr. Giovanni Macelloni
Earth Observation Department
Istituto di Fisica Applicata (IFAC)
Consiglio Nazionale delle Ricerche
Via Madonna del piano 10 - 50019 -Sesto Fiorentino (Fi) - Italy
Tel. + 39 055 5226495 – Fax + 39 055 5226467
E-mail: G.Macelloni@ifac.cnr.it

2 EQUIPMENT

2.1 Instrument description.

The measurements were carried out with IFAC microwave radiometer called RADOMEX, please refers to the Year report 2014 of the project for more information.

2.2 Platform (Satellite, Aircraft, Ground).

Ground

2.3 Key variables.

Microwave brightness temperature at 1.4 GHz (L-band), horizontal and vertical polarization, Infrared temperature (8-14 μm).

2.4 Instrument measurement geometry.

Data were collected from the tower-mounted radiometer from December 2013 to December 2014 at different incidence angles within the 20° - 130° range with respect to nadir (i.e. 0° = nadir view) in the North-West direction. Different procedure have been followed for the acquisition as described in the Final Report and in the Experiment Support Plan of the project.

2.5 Manufacturer of instrument.

Instruments were designed and developed at IFAC CNR Firenze Italy

2.6 Calibration.

Calibration procedure was described in DOMEX-2 –Final report.

3 PROCEDURE

3.1 Data acquisition methods.

Data were collected automatically from the tower-mounted radiometer 24 hours/day. Data acquisition and platform movement were automatically controlled by means of a PC placed in the box; and the experiment was monitored remotely using a Local Area Network connection.

The following parameters were used for the acquisitions:

Integration time (measurement and calibration): 4 second

Number of measurements between calibration: 8 (4 H and 4 V)

Measurement Time (for each position): variable

IMPORTANT NOTE : In the dataset is represented the number of measurements, Tb mean value and standard deviation collected at each single position.

3.2 Spatial characteristics.

3.2.1 Spatial coverage.

Data were acquired at a fixed position at,:

Coordinates: 75.0989°S 123.3005°E

Altitude: 3250 M

The antenna foot-print (HPBW) ranged from 10x14 m² at $\theta = 20^\circ$ to 10 x 160 m² at $\theta = 70^\circ$.

3.2.2 Spatial resolution.

Please refers to Experiment Implementation Plan

3.2.3 Temporal characteristics.

Please refers to Experiment Implementation Plan

3.2.4 Temporal coverage.

Data represented in this dataset were acquired from December 2013 to December 2014

4 DATA DESCRIPTION

4.1 Table definition with comments.

The data base is contained in the file DOMEX_3_SECONDYEAR_2014_MWDATA.txt in ASCII format.

It could be easily opened with MS Excell or Matlab.

The files are composed by a table of 136413 Rows + 1 (header) and 37 Columns

Column description:

c1 = Date – time DD/MM/YY hh:mm

c2 = Number of samples

c3 = Sun zenith position (degs)

c4 = Sun angular position (degs)

c5 = Quality flag; 0 = quality check passed; 1 = quality check not passed
c6 = sun flag; 0 = sun not in front of the antenna; 1 = sun in the antenna pattern
c7 = calibration scheme; 1 = frequent calibration hot and cold load; 2 = frequent calibration fixed gain, cold load; 3 = frequent calibration cold load and noise source.
c8 = TVL= Brightness Temperature L band – Vertical polarization (K)
c9 = Stdev TVL= Standard deviation of #c8 (K)
c10 = THL= Brightness Temperature L band – Horizontal polarization (K)
c11 = Stdev THL= Standard deviation of #c10 (K)
c12 = Theta = Incidence Angle (degrees)
c13 = SdevTheta = Standard deviation of #c12 (degs)
c14 = Theta = Azimuth Angle (degrees)
c15 = SdevTheta = Standard deviation of #c14 (degs)
c16 = Tir= Temperature of the calibrator of IR sensor (°C)
c17 = Stdev Tir= Standard deviation of #c16 (°C)
c18 = Temperature of Tns internal to the Radiometer receiver
c19 = Stdev Tns= Standard deviation of #c18 (°C)
c20 = Temperature of Tsw internal to the Radiometer receiver
c21 = Stdev Tsw= Standard deviation of #c20 (°C)
c22 = Temperature of Tcables1 internal to the Radiometer receiver
c23 = Stdev Tcables= Standard deviation of #c22 (°C)
c24 = Temperature of Tcables1 internal to the Radiometer receiver
c25 = Stdev Tcables= Standard deviation of #c24 (°C)
c26 = Temperature of T_H_omt connector
c27 = Stdev T_H_omt= Standard deviation of #c26 (°C)
c28 = Temperature of T_V_omt connector
c29 = Stdev T_V_omt= Standard deviation of #c28 (°C)
c30 = Temperature of T_H_rad connector
c31 = Stdev T_H_omt= Standard deviation of #c30 (°C)
c32 = Temperature of T_V_rad connector
c33 = Stdev T_V_rad= Standard deviation of #c32 (°C)
c34 = Temperature of T_OMT
c35 = Stdev T_ant= Standard deviation of #c34 (°C)
c36 = Temperature of Antenna front part
c37 = Stdev T_ant= Standard deviation of #c36 (°C)

- Missing data are identified as NaN

5 DATA QUALITY

5.1 Data Manipulations

As described in detail in the DOMEX Final Report the data at L band were processed and calibrated.

5.2 Sources of error.

The errors in the measurement were mainly related to the data post-processing. The adopted procedure is described in the Final Report of the project.

5.3 Quality assessment.

The minimum detectable temperature variation of the radiometer (sensitivity) was 0.3 K (with $\tau = 2$ sec), and the accuracy (repeatability) was better than 0.5 K over a period of 30 days.

6 REFERENCES

Technical Support for the Long-Term Deployment of an L-Band Radiometer at Concordia Station
Yearly Report – First Year Report February 2014 EUROPEAN SPACE AGENCY STUDY
ESTEC Contract 4000105872/12/NL/NF – Macelloni et. al

7 DATA POLICY

The participants (IFAC and CVA) have the exclusive right of access to and exploitation of data lather than 6 months after the end of the project (presentation of the final report). After this date dissemination of the dataset will be performed by ESA under the control and with the approval of IFAC.

TECHNICAL SUPPORT FOR THE LONG-TERM DEPLOYMENT OF AN L-BAND RADIOMETER AT CONCORDIA STATION

DATA DESCRIPTION: SNOWTEMPERATURE

JUNE 2015

EUROPEAN SPACE AGENCY STUDY CONTRACT REPORTS

ESTEC CONTRACT 4000105872/12/NL/NF

PREPARED BY

Giovanni Macelloni, Francesco Montomoli, Simone Pettinato and Marco Brogioni

IFAC – CNR – SESTO FIORENTINO – ITALY

DATE:

June 2015



This page is intentionally left blank

ESA STUDY CONTRACT REPORT			
EUROPEAN SPACE AGENCY STUDY CONTRACT REPORTS ESTEC CONTRACT 4000105872/12/NL/NF	TECHNICAL SUPPORT FOR THE LONG- TERM DEPLOYMENT OF AN L-BAND RADIOMETER AT CONCORDIA STATION	CONTRACTOR: IFAC-CNR	
ESA CR ()No:	STAR CODE:	No of volumes: 1 This is volume no: 1	CONTRACTOR'S REF: Snow Temperature DataBase
<p>ABSTRACT:</p> <p>This report contains the information of the snow temperature data collected during DOMEX-3 experiment.</p>			
<p>The work described in this report was done under ESA Contract. Responsibility for the contents resides in the author or organisation that prepared it.</p>			
<p>AUTHORS: G. Macelloni, F.Montomoli, M. Brogioni, S.Pettinato (IFAC-CNR)</p>			
<p>ESA STUDY MANAGER: T.Casal</p>		<p>ESA BUDGET HEADING</p>	

This page is intentionally left blank

1 TITLE

1.1 Data set identification

DOMEX-3 Snow Temperature Data

1.2 Revision date of this document (yyyy/mm/dd)

2015/06/12

2 INVESTIGATOR(S)

Dr. Giovanni Macelloni
Earth Observation Department
Istituto di Fisica Applicata (IFAC)
Consiglio Nazionale delle Ricerche
Via Madonna del piano 10 - 50019 -Sesto Fiorentino (Fi) - Italy
Tel. + 39 055 5226495 – Fax + 39 055 5226467
E-mail: G.Macelloni@ifac.cnr.it

3 EQUIPMENT

3.1 Instrument description.

The measurements were carried out with LSI LASTEM –data logger. –Model EL 305 and EL 105,
Probes: PT100 Din-A
Please refers to <http://www.lsi-lastem.it> for more information.

3.2 Platform (Satellite, Aircraft, Ground).

Ground

3.3 Key variables.

Snow Temperature measured at different depth (range 0-10 m)

3.4 Instrument measurement geometry.

The temperature profile of the first 10 m of the snow pack was measured by using 10 probes. The probes (PT100 –DIN-A) were placed at different depths as described Table 1Table .

Table 1

Probe N	Depth (cm)
1	5
2	10
3	25
4	50
5	100
6	150
7	200
8	250
9	300
10	400
11	500
12	600
13	800
14	1000

3.5 Manufacturer of instrument.

Instruments were designed and developed by LSI-LASTEM (Italy).

4 PROCEDURE

4.1 Data acquisition methods.

Data were collected automatically by the data logger.

Data were acquired at each minute and recorded at each hour (mean, maximum, minimum).

IMPORTANT NOTE : In the dataset is represented the mean value are represented, the typical value of the standard deviation is less than 0.05 °C, maximum value is 0.1 °C

4.2 Spatial characteristics.

Spatial coverage.

Data were acquired at a fixed position at,:

Coordinates: 75.0989°S 123.3005°E

Altitude: 3250 M

Please refers to the Final Report of the project for more information

4.3 Temporal characteristics.

Temporal coverage.

Data represented in this dataset were acquired from January2014 to May 2015.

Because of some problems affected the acquisition system, in some periods data were not collected. Please refers to the Final Report of the project for more information

5 5. DATA DESCRIPTION

5.1 Table definition with comments.

The data base is contained in the file **DOMEX3_snowtemp_database2.txt** as ASCII format.

It could be easily opened with MS Excel or Matlab.

The file is composed by a table 11740 rows + 1 (header) and 46 Columns.

Columns description:

c1 =Date – time YYYYMMDDTHHMMSS

c2 = T1= Minimum Temperature Probe 1 (50 cm) (°C)

c3 = T1= Mean Temperature Probe 1 (50 cm) (°C)

c4 = T1= Maximum Temperature Probe 1 (50 cm) (°C)

c5 = T2= Minimum Temperature Probe 1 (10 cm) (°C)

c6 = T2= Mean Temperature Probe 1 (10 cm) (°C)
c7 = T2= Maximum Temperature Probe 1 (10 cm) (°C)
c8 = T3= Minimum Temperature Probe 1 (100 cm) (°C)
c9 = T3= Mean Temperature Probe 1 (100 cm) (°C)
c10 = T3= Maximum Temperature Probe 1 (100 cm) (°C)
c10 = T4= Minimum Temperature Probe 1 (800 cm) (°C)
c11 = T4= Mean Temperature Probe 1 (800 cm) (°C)
c12 = T4= Maximum Temperature Probe 1 (800 cm) (°C)
c13 = T5= Minimum Temperature Probe 1 (600 cm) (°C)
c14 = T5= Mean Temperature Probe 1 (600 cm) (°C)
c15 = T5= Maximum Temperature Probe 1 (600 cm) (°C)
c16 = T6= Minimum Temperature Probe 1 (400 cm) (°C)
c17 = T6= Mean Temperature Probe 1 (400 cm) (°C)
c18 = T6= Maximum Temperature Probe 1 (400 cm) (°C)
c19 = T7= Minimum Temperature Probe 1 (300 cm) (°C)
c20 = T7= Mean Temperature Probe 1 (300 cm) (°C)
c21 = T7= Maximum Temperature Probe 1 (300 cm) (°C)
c22 = T8= Minimum Temperature Probe 1 (500 cm) (°C)
c23 = T8= Mean Temperature Probe 1 (500 cm) (°C)
c24 = T8= Maximum Temperature Probe 1 (500 cm) (°C)
c25 = T10= Minimum Temperature Probe 1 (5 cm) (°C)
c26 = T10= Mean Temperature Probe 1 (5 cm) (°C)
c27 = T10= Maximum Temperature Probe 1 (5 cm) (°C)
c28 = T11= Minimum Temperature Probe 1 (1000 cm) (°C)
c29 = T11= Mean Temperature Probe 1 (1000 cm) (°C)
c30 = T11= Maximum Temperature Probe 1 (1000 cm) (°C)
c31 = T12= Minimum Temperature Probe 1 (25 cm) (°C)
c32 = T12= Mean Temperature Probe 1 (25 cm) (°C)
c33 = T12= Maximum Temperature Probe 1 (25 cm) (°C)
c34 = T13= Minimum Temperature Probe 1 (150 cm) (°C)
c35 = T13= Mean Temperature Probe 1 (150 cm) (°C)
c36 = T13= Maximum Temperature Probe 1 (150 cm) (°C)
c37 = T14= Minimum Temperature Probe 1 (250 cm) (°C)
c38 = T14= Mean Temperature Probe 1 (250 cm) (°C)
c39 = T14= Maximum Temperature Probe 1 (250 cm) (°C)
c40 = T15= Minimum Temperature Probe 1 (200 cm) (°C)
c41 = T15= Mean Temperature Probe 1 (200 cm) (°C)
c42 = T15= Maximum Temperature Probe 1 (200 cm) (°C)
c43 = T16= Minimum Temperature Probe 1 (75 cm) (°C)
c44 = T16= Mean Temperature Probe 1 (75 cm) (°C)
c45 = T16= Maximum Temperature Probe 1 (75 cm) (°C)

- Missing data are identified as NaN

6 DATA QUALITY

6.1 Data Manipulations

Data were not manipulated

7 Sources of error.

Please refers to LSI-Lastem information

8 Quality assessment.

Please refers to LSI-Lastem information

9 REFERENCES

[1] LSI-LASTEM user manual (<http://www.lsi-lastem.it/pdf/instum00031.pdf>)

[2] TECHNICAL SUPPORT FOR THE LONG-TERM DEPLOYMENT OF AN L-BAND RADIOMETER AT
CONCORDIA STATION

10 DATA POLICY

The participants (IFAC and CVA) have the exclusive right of access to and exploitation of data lather than 6 months after the end of the project (presentation of the final report). After this date dissemination of the dataset will be performed by ESA under the control and with the approval of IFAC.